Observation of non-Abelian Anderson localization and transition in topolectrical circuits

Haiteng Wang,[1] Weixuan Zhang,[1,*] Houjun Sun,[2] and Xiangdong Zhang [1]

[1]*Key Laboratory of Advanced Optoelectronic Quantum Architecture and Measurements of Ministry of Education, Beijing Key Laboratory of Nanophotonics & Ultrafine Optoelectronic Systems, School of Physics, Beijing Institute of Technology, 100081 Beijing, China*
[2]*Beijing Key Laboratory of Millimeter wave and Terahertz Techniques, School of Information and Electronics, Beijing Institute of Technology, Beijing 100081, China*

Anderson localization, which originates from the wave interference between multiple-scattering paths, has been widely explored in quantum and classical systems with disordered Abelian gauge potentials. Recently, the interplay between disorder and non-Abelian gauge fields has been theoretically investigated, revealing non-Abelian Anderson localization and transition without Abelian analogy. Due to the limitation on engineering non-Abelian gauge potentials with disorder, the experimental observation of non-Abelian Anderson phenomena is still lacking. Here, we report on the experimental realization of non-Abelian Anderson localization and transition based on engineered topolectrical circuits, which are directly mapped to the quasiperiodic Aubry-André Harper model with non-Abelian gauge fields. Disorder can be suitably introduced into the effective non-Abelian coupling matrices by randomly setting the values of coupling and grounding circuit elements. In this case, different types of non-Abelian Anderson phases, including the delocalization phase, coexisting states with localized and delocalized spatial profiles, and the localization phase, can be clearly observed by measuring the site-resolved impedance spectra and voltage dynamics. Our proposal provides a flexible platform to investigate Anderson localization and transition driven by non-Abelian gauge potentials with disorder and could have potential applications in the electronic signal control.

I. INTRODUCTION

Anderson localization [1], which is a ubiquitous wave phenomenon arising from the destructive interference of waves scattered off by uncorrelated static disorder, has been widely realized in many artificial systems, including ultracold atoms [2–6], photonics [7–17], ultrasound wave [18,19], electrical circuits [20], and so on [21–24]. Except for Anderson localization in disordered systems, the Aubry-André-Harper (AAH) model [25,26], a paradigmatic example of a one-dimensional (1D) quasicrystal, with a truly incommensurate potential can undergo a sudden metal-insulator phase transition at a critical strength of the quasiperiodic potential [27–30]. At the critical point, the AAH model can be reduced to the Harper equation, which can be mapped onto the two-dimensional (2D) Hofstadter model on a square lattice with a nontrivial topology [31–34]. In recent years, the 1D AAH model has been experimentally realized in many classical systems; both metal-insulator phase transition and topological edge states have been directly observed. In addition, the topological triple-phase transition, where the changing of a single parameter simultaneously gives rise to the metal-insulator transition, topological phase transition, and the parity-time symmetry phase transition, was theoretically proposed and experimentally realized [35–40]. Investigations of Anderson localization and transition of the 1D AAH model, especially in

the experimental aspect, are mainly focused on systems with quasiperiodic Abelian gauge potentials.

Different from the Abelian gauge field, Yang and Mills [41] proposed the concept of non-Abelian gauge fields, which leverage the internal degrees of freedom of particles, to describe the interaction between nucleons. Recently, researchers have extended the non-Abelian gauge fields into real spaces and parameter spaces, giving opportunities to explore non-Abelian physics in artificial systems, such as cold atoms [42], exciton-polaritons [43–46], mechanics and acoustics [47–49], electrical circuits [50,51], and photonics [52,53]. For example, the multiple-band topology has been revealed using non-Abelian topological charges [54], and the non-Abelian braiding has also been realized in some photonic and acoustic structures [55,56]. Non-Abelian Anderson localization and transition have also been theoretically investigated using the 1D AAH model with non-Abelian gauge potentials [57]. However, due to the limitation on engineering disordered non-Abelian gauge potentials, experimental observations of non-Abelian Anderson localizations and metal-insulator transitions are still lacking.

In this paper, we report on the experimental realization of non-Abelian Anderson localization and transition based on engineered topolectrical circuits. By mapping eigenmodes of the 1D non-Abelian AAH model to the modes of designed electrical circuits, non-Abelian Anderson localization and metal-insulator transition can be realized. Based on the flexibly of circuit connections and groundings, different strengths of disorder can be easily implemented in the non-Abelian

*zhangwx@bit.edu.cn

AAH circuits. In this case, different types of non-Abelian Anderson phases, including the delocalization phase, coexisting states with localized and delocalized eigenstates, and the localization phase, can be clearly observed by measuring the site-resolved impedance spectra and voltage dynamics. In this paper, we suggest a way to investigate the interplay between disorder, non-Abelian gauge potentials, and metal-insulator transitions, which could have potential applications in electronic signal control.

II. THEORY OF NON-ABELIAN ANDERSON LOCALIZATION AND TRANSITION IN ELECTRICAL CIRCUITS

We consider a 1D non-Abelian AAH quasiperiodic model, as shown in Fig. 1(a). Each lattice site contains two internal degrees of freedom, providing a pair of pseudospins of $|\uparrow\rangle = [1, 0]^T$ and $|\downarrow\rangle = [0, 1]^T$. The coupling matrix between adjacent sites is marked by M. Meanwhile, the quasiperiodic onsite modulation U_n is applied to the non-Abelian AAH model. In this case, the Hamiltonian of the system with open boundaries can be written as

$$H = \sum_{n=1}^{N} (\psi_n^+ U_n \psi_n) + \sum_{n=2}^{N-1} (\psi_{n+1}^+ M \psi_n + \psi_{n-1}^+ M^+ \psi_n), \quad (1)$$

where $\psi_n^+ = [\psi_{n,\uparrow}^+, \psi_{n,\downarrow}^+]$ $(\psi_n = [\psi_{n,\uparrow}, \psi_{n,\downarrow}]^T)$ is the two-component creation (annihilation) operator at the site n. Here, N is the total number of the lattice sites. We set the coupling matrix in the form of $M = \begin{bmatrix} \cos(q) & \sin(q) \\ -\sin(q) & \cos(q) \end{bmatrix}$, with q determining the coupling strength. In addition, the on-site modulation matrix is written as $U_n = 2J \begin{bmatrix} \cos(q)\cos(2\pi\chi n) & -\sin(q)\sin(2\pi\chi n) \\ -\sin(q)\sin(2\pi\chi n) & \cos(q)\cos(2\pi\chi n) \end{bmatrix}$ at the nth site, where J is the modulation strength and χ is an irrational number to introduce the quasiperiodic modulation. In the following, we set $q = 0.3\pi$ and $\chi = (\sqrt{5}-1)/2$. The wave function in the non-Abelian AAH model can be expressed as $|\Psi\rangle = \sum_{n=1}^{N} [\varphi_{\psi_{n,\uparrow}}, \varphi_{\psi_{n,\downarrow}}][\psi_{n,\uparrow}^+, \psi_{n,\downarrow}^+]^T|0\rangle$, where $\varphi_{\psi_{n,\uparrow}}$ $(\varphi_{\psi_{n,\downarrow}})$ represents the probability amplitude of $|\uparrow\rangle$ $(|\downarrow\rangle)$ on the nth lattice site. Solving the steady-state Schrödinger equation $H|\Psi\rangle = \varepsilon|\Psi\rangle$, the eigenequation of the system can be described by

$$\varepsilon \begin{pmatrix} \varphi_{\psi_{n,\uparrow}} \\ \varphi_{\psi_{n,\downarrow}} \end{pmatrix} = M \begin{pmatrix} \varphi_{\psi_{n+1,\uparrow}} \\ \varphi_{\psi_{n+1,\downarrow}} \end{pmatrix} + M^+ \begin{pmatrix} \varphi_{\psi_{n-1,\uparrow}} \\ \varphi_{\psi_{n-1,\downarrow}} \end{pmatrix} + U_n \begin{pmatrix} \varphi_{\psi_{n,\uparrow}} \\ \varphi_{\psi_{n,\downarrow}} \end{pmatrix}. \quad (2)$$

We note that the experimental realization of such a 1D non-Abelian AAH model is not an easy task, which requires the non-Abelian modulation of both site couplings and the on-site potential. How to construct a suitable platform to simulate this system is still an open question. Based on the similarity between circuit Laplacian and lattice Hamiltonian [20,50,51,58–83], electrical circuits can be used as an ideal platform to achieve the 1D non-Abelian AAH model. The schematic diagram for a unit cell of the designed electrical circuit is shown in Fig. 1(b). Here, to realize the non-Abelian coupling matrix, a pair of circuit nodes connected by the capacitor C are considered to form an internal degree at each lattice site. Voltages at these two nodes are expressed as V_{1,n_σ} and V_{2,n_σ} $(\sigma = |\uparrow\rangle, |\downarrow\rangle,$ and $n = 1, 2, ..., N)$. In this case, we can construct two decoupled sectors $V_{A,n_\sigma} =$

$(V_{1,n_\sigma} - V_{2,n_\sigma})/\sqrt{2}$ and $V_{S,n_\sigma} = (V_{1,n_\sigma} + V_{2,n_\sigma})/\sqrt{2}$ of designed electrical circuits, where the effective coupling of the antisymmetric sector V_A can be mapped to non-Abelian AAH model. The negative (positive) intersite coupling of $-\cos(q)$ and $-\sin(q)$ [$\cos(q)$ and $\sin(q)$] can be realized by connecting two node pairs by the capacitor $C_c = C\cos(q)$ and $C_s = C\sin(q)$ with (without) a cross. To realize the non-Abelian on-site modulation, two node pairs belonging to the same lattice site are needed to be suitably connected and grounded. Specifically, the positive (negative) nondiagonal elements in the modulation matrix U_n can be constructed by connecting two node pairs at the nth site through the site-dependent capacitors $C_{n'} = 2C_J\sin(q)\sin(2\pi\chi n)$ without (with) a cross. The diagonal elements of U_n are realized by grounding circuit nodes with site-dependent capacitors $C_n = 2C_J\cos(q)\cos(2\pi\chi n)$. In addition, there are some negative values of C_n at different circuit nodes due to the cosine modulation. To eliminate the appearance of negative values of C_n, we ground a constant capacitor C_u at each node (equivalent to adding a constant potential in the non-Abelian AAH model). It is noted that the added constant potential does not influence the phase transition properties of the non-Abelian AAH model. In this case, the diagonal elements of the effective potential matrix $\begin{bmatrix} C_u + 2C_J\cos(q)\cos(2\pi\chi n) & -2C_J\sin(q)\sin(2\pi\chi n) \\ -2C_J\sin(q)\sin(2\pi\chi n) & C_u + 2C_J\cos(q)\cos(2\pi\chi n) \end{bmatrix}$ are always larger than zero, so that the quasiperiodic grounding capacitor $C_u + 2C_J\cos(q)\cos(2\pi\chi n)$ is positive at each node. Each circuit node is also grounded by an inductor L_g. Through the appropriate setting of grounding and connecting, the circuit eigenequation can be derived as

$$\left(\frac{f_0^2}{f^2} - 2 - 2\frac{C_c}{C} - 2\frac{C_s}{C} - \frac{C_u}{C} - \frac{C_{n'}}{C} \right) \begin{vmatrix} V_{A,n\uparrow} \\ V_{A,n\downarrow} \end{vmatrix}$$
$$= -\left(\begin{bmatrix} \frac{C_c}{C} & \frac{C_s}{C} \\ -\frac{C_s}{C} & \frac{C_c}{C} \end{bmatrix} \begin{vmatrix} V_{A,n+1\uparrow} \\ V_{A,n+1\downarrow} \end{vmatrix} + \begin{bmatrix} \frac{C_c}{C} & -\frac{C_s}{C} \\ \frac{C_s}{C} & \frac{C_c}{C} \end{bmatrix} \begin{vmatrix} V_{A,n-1\uparrow} \\ V_{A,n-1\downarrow} \end{vmatrix} \right)$$
$$+ \begin{bmatrix} \frac{C_n}{C} & -\frac{C_{n'}}{C} \\ -\frac{C_{n'}}{C} & \frac{C_n}{C} \end{bmatrix} \begin{vmatrix} V_{A,n\uparrow} \\ V_{A,n\downarrow} \end{vmatrix}, \quad (3)$$

where f is the eigenfrequency ($f_0 = 1/2\pi\sqrt{L_gC}$) of the designed electrical circuit. Details for the derivation of circuit eigenequations are provided in Appendix A. It is shown that the eigenequation of the designed electrical circuit possesses the same form as Eq. (1). The probability amplitudes for the 1D non-Abelian AAH model $\varphi_{\psi_{n,\uparrow}}$ and $\varphi_{\psi_{n,\downarrow}}$ are mapped to the voltages of pseudospins $V_{A,n\uparrow}$ and $V_{A,n\downarrow}$. The eigenfrequency of the circuit is related to the eigenenergy in the form of $\varepsilon = \frac{f_0^2}{f^2} - 2 - 2\frac{C_c}{C} - 2\frac{C_s}{C} - \frac{C_u}{C} - \frac{C_{n'}}{C}$. The effective non-Abelian matrices are given by $M = \begin{bmatrix} \frac{C_c}{C} & \frac{C_s}{C} \\ -\frac{C_s}{C} & \frac{C_c}{C} \end{bmatrix}$ and $U_n = \begin{bmatrix} \frac{C_n}{C} & -\frac{C_{n'}}{C} \\ -\frac{C_{n'}}{C} & \frac{C_n}{C} \end{bmatrix}$. In this case, we have achieved the above-proposed non-Abelian AAH model in electrical circuits. The strength of disorder on the on-site modulation matrix can be changed by adjusting the value of C_J.

To investigate the Anderson transitions in the designed non-Abelian AAH circuits, we calculate the inverse participation ratio IPR $= \sum_{n=1}^{N} |V_{A,n_\sigma}|^4 / \left(\sum_n |V_{A,n_\sigma}|^2 \right)^2$ of all eigenstates for the designed electrical circuit with different
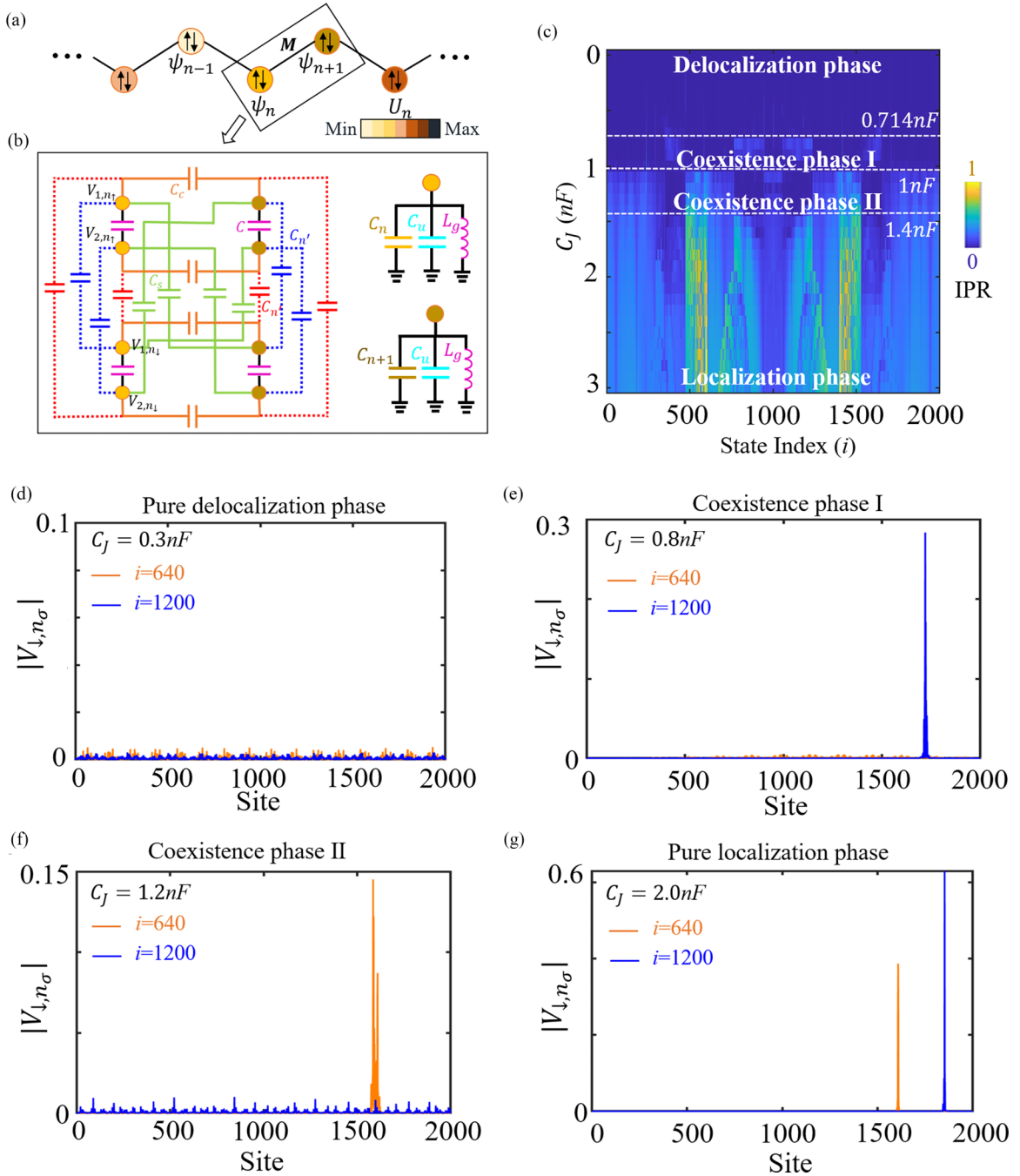
FIG. 1. Numerical results on the non-Abelian Anderson localization in electrical circuits. (a) Schematic diagram of the one-dimensional (1D) non-Abelian Aubry-André-Harper (AAH) quasiperiodic model. Each lattice site contains two internal degrees of freedom marked by $|\uparrow\rangle$ and $|\downarrow\rangle$. M represents the coupling matrix between two adjacent sites. U_n defines the onsite modulation matrix of site n. (b) Illustrations of the non-Abelian hopping matrix in electrical circuits between two sites enclosed by the black block in (a). The grounding capacitors and inductors are shown in the right inset. (c) The calculated inverse participation ratio (IPR) of the non-Abelian AAH circuit vs the strength of disorder (C_J). Four regimes separated by three critical values of $C_J = 0.714nF$, $1.4nF$, and $1nF$ correspond to the delocalization phase, the coexistence phase I, the coexistence phase II, and localization phase, respectively. Other circuit parameters are set as $C = 1nF$, $L_g = 33uH$, $C_u = 2.5nF$. (d)–(g) Spatial profiles of two eigenstates of $i = 640$ (the orange line) and $i = 1200$ (the blue line) with disorder strength being $C_J = 0.3nF$, $0.8nF$, $1.2nF$, and $2.0nF$.

values of C_J in the range of $[0nF, 3nF]$. It is noted that the IPR of an extended state is extremely small, while it remains finite for a localized state. In the following calculation, other circuit parameters are set as $C = 1nF$, $L_g = 33uH$, and $C_u = 2.5nF$, respectively. Obviously, the IPR phase diagram

in Fig. 1(c) provides four regimes separated by three critical values of $C_J = 0.714nF$, $1.4nF$, and $1nF$ (marked by three white lines). When the strength of disorder (C_J) is sufficiently small ($<0.714nF$), the values of calculated IPRs are approximately vanishing for all eigenstates, indicating all eigenstates

TABLE I. A few representative examples on capacitances.

	Formula	Precision values	Finite precision	Realization
C_c	$C\cos(0.3\pi)$	$0.5878nF$	$0.59nF$	$470pF + 120pF$
C_S	$C\sin(0.3\pi)$	$0.8090nF$	$0.81nF$	$820pF$
C_n	$2C_J\cos(q)\cos(2\pi\chi n)$	$1.4305nF$ $(n = 2)$	$1.43nF$	$1nF + 430pF$
$C_{n'}$	$2C_J\sin(q)\sin(2\pi\chi n')$	$2.5681nF$ $(n' = 2)$	$2.57nF$	$2nF + 470pF + 100pF$
C_u	C_u	$2.5nF$	$2.5nF$	$2nF + 470pF + 30pF$
L_g	L_g	$33uH$	$33uH$	$33uH$

are extended states, and the non-Abelian AAH circuit is in the delocalization phase. Figure 1(d) presents spatial profiles of two eigenstates of $i = 640$ and 1200 (i is the state index) with $C_J = 0.3nF$. It is clearly shown that these two eigenstates exhibit extended spatial distributions. Two types of coexistence phases—that is, the localized and extended states can be found at the same disorder strength—emerge within the regime from $0.714nF$ to $1.4nF$. These two coexistence phases are separated by the critical value of $C_J = 1nF$. We mark these two phases as coexistence phases I and II. In Figs. 1(e) and 1(f), the spatial profiles of two eigenstates ($i = 640$ and 1200) are plotted with $C_J = 0.8nF$ and $1.2nF$, respectively. We find that one eigenstate of $i = 1200$ (640) exhibits the strong localization and the other eigenstate of $i = 640$ (1200) is delocalized in the whole structure with $C_J = 0.8nF$ ($1.2nF$), indicating the appearance of coexistence phase in the quasiperiodic non-Abelian AAH circuit. As C_J further increases to a value $>1.4nF$, the system enters the localization phase verified by the large value of IPRs for all eigenstates. The calculated spatial profiles of two eigenstates ($i = 640$ and 1200) further confirm that the system enters the localization phase with $C_J = 2.0nF$, as shown in Fig. 1(g). Above numerical results clearly show that the non-Abelian Anderson transition from delocalized states to coexistence phases and from coexistence phases to localized states can be realized in our designed non-Abelian AAH circuits with different strengths of disorder on the modulation matrix.

III. EXPERIMENTAL OBSERVATION OF NON-ABELIAN ANDERSON LOCALIZATION AND TRANSITION IN ELECTRICAL CIRCUITS

To experimentally observe non-Abelian Anderson localization and transition, the designed non-Abelian AAH circuits are fabricated. The photographic image of two coupled sites for the circuit sample is displayed in the left chart of Fig. 2(a). The right chart shows the photo of grounding at two sites. Here, the capacitor C (marked by pink) is used to connect a pair of circuit nodes to construct an internal degree at each site. The adjacent node pairs are connected by capacitors C_c and C_s (marked by orange and green) with (without) a cross to realize the negative (positive) intersite coupling. In addition, the positive (negative) nondiagonal elements in the modulation matrix U_n can be fulfilled by coupling node pairs (belonging to two internal degrees at a single site) through the capacitor $C_{n'}$ marked by blue (red) without (with) a cross. The grounding inductor L_g and capacitor C_n are enclosed by pink and yellow (brown) frames in the right chart. In addition, as circled by cyan squares, the extra capacitors C_u

are used to complement the negative grounding capacitor C_n. The whole photograph images for the circuit samples with different strengths of disorder are shown in Appendix B. The values of C, L_g, and C_u are the same as that used in Fig. 1(c). It is important to note that the realization of capacitors with precise values is very hard by factory-made capacitors. Here, we take two decimal places of applied capacitances in experiments, where the phase transition of non-Abelian AAH model still exists. In this case, the finite-precision capacitances can be experimentally realized by factory-made capacitors with series connections. Table I illustrates some representative examples.

To observe non-Abelian Anderson transition and localization, we measure impedance spectra of two nodes in the non-Abelian AAH circuits with different disorder strengths. It is noted that the eigenfrequency and eigenmodes of voltages have a one-to-one correspondence to the eigenenergy and eigenstates of the mapped lattice model. Moreover, the circuit impedance equals the ratio of voltage and current. Hence, the impedance response of a circuit node is related to the local amplitude of eigenstate for the mapped lattice model. In this case, the measurement of impedance spectrum in the frequency domain can reflect the local amplitudes of wave function at different eigenenergies that are related to local density of states for the mapped lattice model. Here, we excite the circuit in the pseudospin subspace of $|\uparrow\rangle$, and the impedance spectra in the other pseudospin subspace of $|\downarrow\rangle$ possess similar properties (see Appendix C). The blue and orange lines in Fig. 2(b) present the experimental results of impedance spectra at two circuit nodes of $n = 24$ and 70 (shown in Fig. 3) with $C_J = 0.3nF$, which stays in the range of delocalization phase. It is found that there are many impedance peaks at different frequencies from 0.25 to 0.55 MHz, manifesting the extension of eigenspectra for the non-Abelian AAH circuit. In addition, the peak values are extremely small, consistent with the delocalized eigenfields in the circuit with $C_J = 0.3nF$. Then we change the disorder strength to $C_J = 0.8nF$ and measure the impedance spectra at these two nodes, as shown in Fig. 2(c). It is clearly shown that the impedance responses at different circuit nodes displays completely opposite phenomena. There is a large-valued impedance peak (the blue line) located at 0.44 MHz at the node $n = 24$. Differently, it is found that lots of impedance peaks with small values appear (the orange line) when the other circuit node with $n = 70$ is excited. These phenomena are consistent with the property of coexistence phase I, showing that delocalized and localized eigenstates coexist in the non-Abelian AAH circuit. Furthermore, Fig. 2(d) displays the impedance responses of two circuit nodes with $C_J = 1.2nF$ that belong to coexistence phase II. In
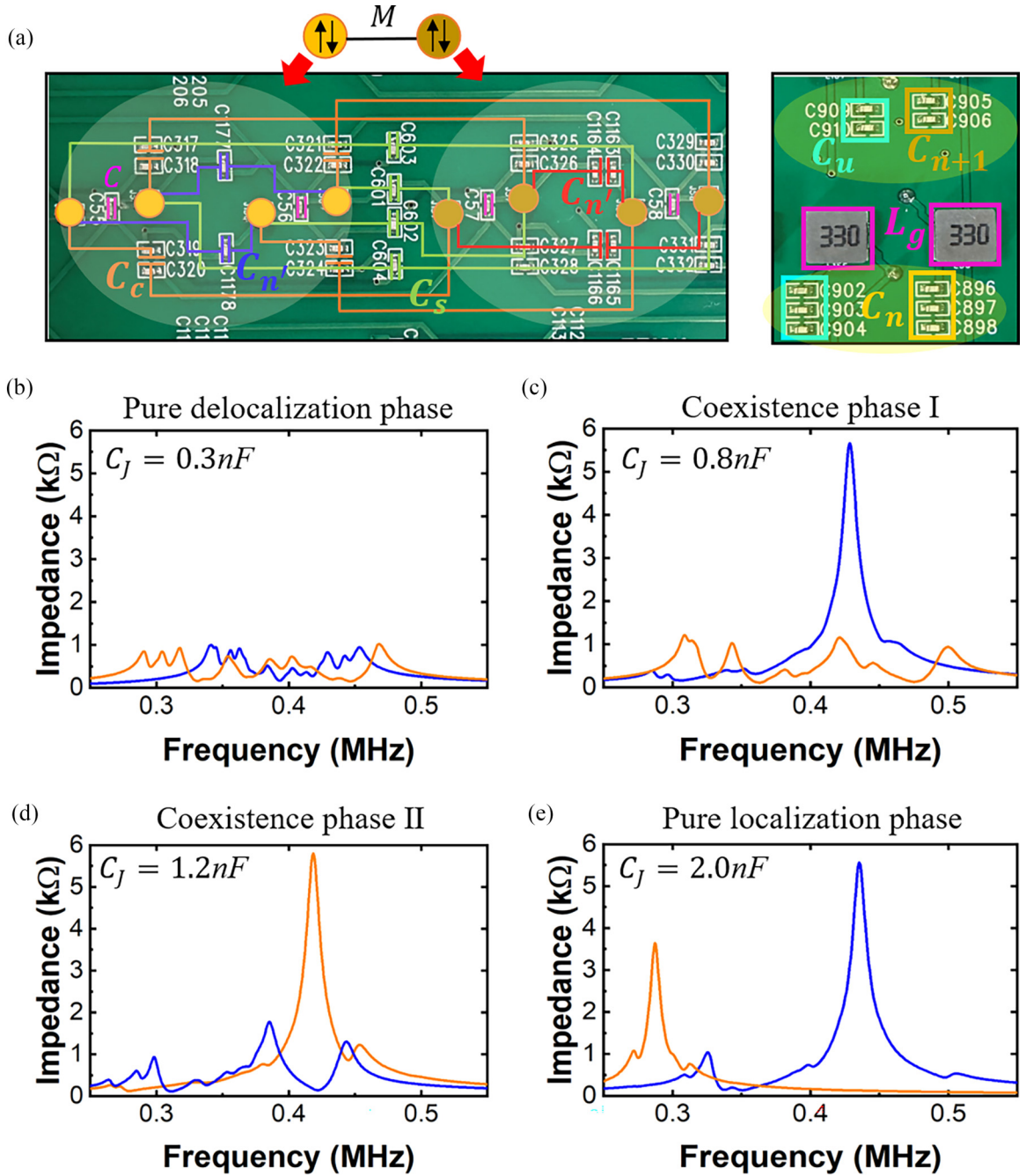
FIG. 2. Experimental observation of non-Abelian Anderson localization and transition in electrical circuits. (a) The photographic image of two coupled sites in the fabricated one-dimensional (1D) non-Abelian Aubry-André-Harper (AAH) circuit. Right and left charts present the realization of non-Abelian coupling matrix and on-site potential, respectively. (b) Measured impedance responses in the pseudospin subspace of $|\uparrow\rangle$ with $C_J = 0.3nF$, which correspond to the delocalization phase. (c) and (d) Measured impedance spectra of 1D non-Abelian AAH circuits staying in the coexistence phases I and II, respectively, where the strengths of disorder are quantified by $C_J = 0.8nF$ and $1.2nF$, respectively. (e) Measured impedance responses with $C_J = 2.0nF$, corresponding to the localization phase of the non-Abelian AAH circuit. The blue and orange lines represent impedance spectra at two different circuit nodes of $n = 24$ and 70.

contrast to the result of coexistence phase I, it is shown that the impedance spectrum of circuit node ($n = 70$) marked by the orange line exhibits a large-valued impedance peak at 0.42 MHz, but the other circuit node ($n = 24$, illustrated by the blue line) shows many impedance peaks with small values. These results clearly manifest the characteristics of eigenstates in coexistence phase II. Due to the self-duality

of the model, the eigenstates that are delocalized in coexistence phase I are localized in coexistence phase II and vice versa. In addition, the existence of dualities in 1D quasiperiodic systems arises quite generically, even for models that are not exactly self-dual [84]. Therefore, dualities between extended and localized states can exist even in the presence of circuit imperfections. By further increasing the disorder
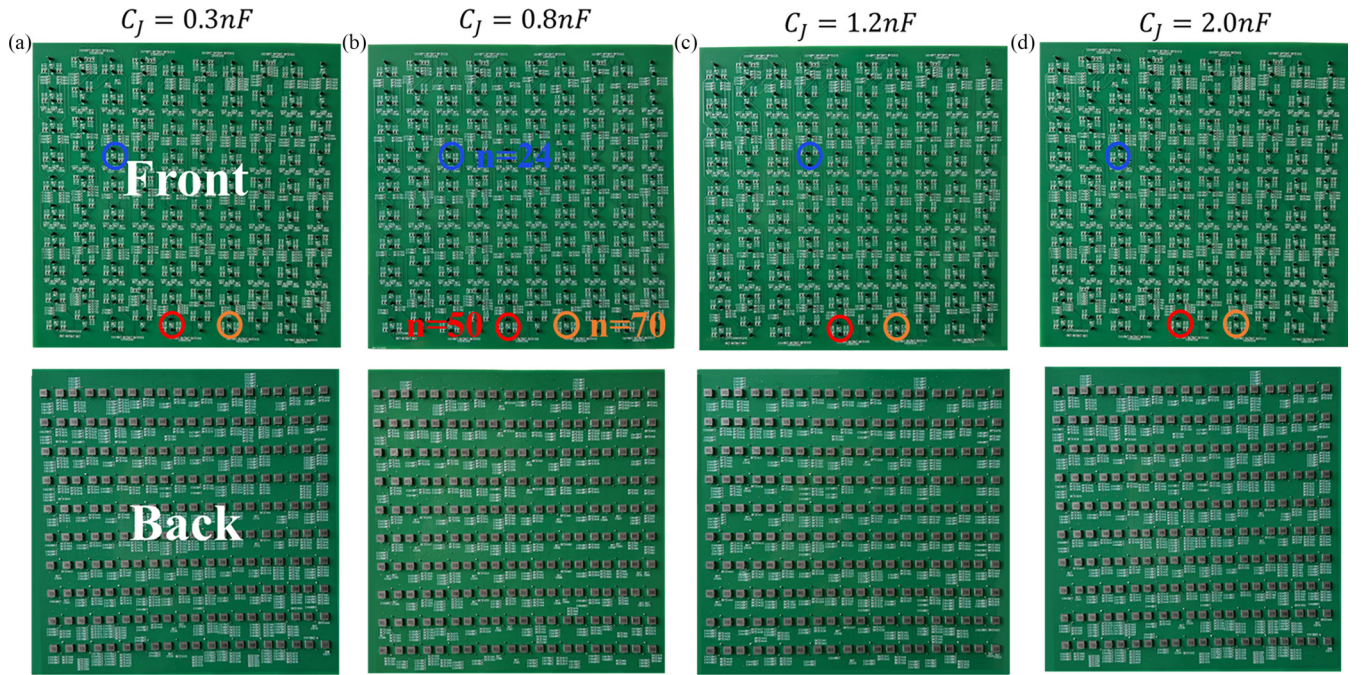
FIG. 3. Photograph images of fabricated circuits. (a)–(d) The front and back sides of photograph images for the fabricated circuits with $C_J = 0.3nF$, $0.8nF$, $1.2nF$, and $2.0nF$. The blue and orange circles with $n = 24$ and 70 mark circuit nodes with measured impedance spectra. The red circles indicate the excited nodes during voltage dynamics measurement.

strength to $C_J = 2.0nF$ (belonging to the localization phase), the measured impedance spectra at two circuit nodes $n = 24$ and 70 show the large-valued impedance peaks at 0.29 and 0.44 MHz, as presented in Fig. 2(e). This phenomenon demonstrates that the non-Abelian AAH circuit goes in the localization phase. The corresponding simulation results of impedance responses for non-Abelian AAH circuits with four different disorder strengths are given in Appendix D. Good consistency between simulations and measurements is obtained, and the larger width of measured impedance peaks should result from the lossy effect in fabricated circuits. The above experimental results clearly demonstrate the observation of non-Abelian Anderson transition from delocalized states to coexistence phases and from coexistence phases to localized states by four 1D non-Abelian AAH circuits with different disorder strengths. In Appendix D, the impedance spectra of two types of electrical circuits, where one precisely matches the quasiperiodic distribution and the other slightly deviates from the quasiperiodic distribution with finite-precision capacitances, are calculated. It is shown that impedance spectra of these two types of electrical circuits are nearly identical, showing the effectiveness on the implementation of the non-Abelian AAH model with finite-precision capacitances.

To further experimentally demonstrate non-Abelian Anderson transition and localization, we measure the temporal dynamics of the non-Abelian AAH circuits with different disorder strengths. Here, the circuit excitation is in the form of $(V_{1,50_\uparrow} = V_0 e^{i\omega t}, V_{2,50_\uparrow} = -V_0 e^{i\omega t})$, locating at the 50th site (marked in Fig. 3) in the $|\uparrow\rangle$ subspace. Excitation frequencies are matched to that of impedance peaks (in Fig. 2) with different strengths of disorder. The top and bottom charts

in Fig. 4(a) display the measured voltage signals in the non-Abelian AAH circuit with $C_J = 0.3nF$, and the excitation frequencies are 0.35 and 0.45 MHz. We can clearly see that the voltage signals spread quickly at two frequencies, indicating the delocalization effect in the non-Abelian AAH circuit with a low-valued disorder strength. Then we measure the voltage dynamics in the non-Abelian AAH circuit with $C_J = 0.8nF$, as shown in Fig. 4(b). In this case, the excitation frequencies are set as 0.35 and 0.44 MHz, which correspond to two impedance peaks in Fig. 2(c). When the excitation frequency equals 0.35 MHz, the input voltage signal exhibits fast-extension behavior. On the contrary, the injected voltage is localized around the input node at 0.44 MHz. These results demonstrate that the delocalization and localization eigenstates coexist in the non-Abelian AAH circuit, corresponding to the regime of coexistence phase I. As displayed in Fig. 4(c), we further measure the voltage dynamics with the disorder strength being $C_J = 1.2nF$, where the excitation frequencies are 0.42 and 0.38 MHz. It is clearly shown that the input voltage displays a significant localization at 0.42 MHz, but the voltage signals extend quickly with the frequency of the input signal being 0.38 MHz. This is consistent with the characteristics of eigenstates in coexistence phase II. Finally, when the disorder strength increases to $C_J = 2.0nF$, we can clearly observe the strong localization of voltage signals at both excitation frequencies of 0.29 and 0.44 MHz, as shown in Fig. 4(d). In this case, we have achieved the localization phase originating from the strong strength of disorder. These experimental results are consistent with simulation results provided in Appendix E, manifesting the observation of non-Abelian Anderson localization and transition by non-Abelian AAH circuits.
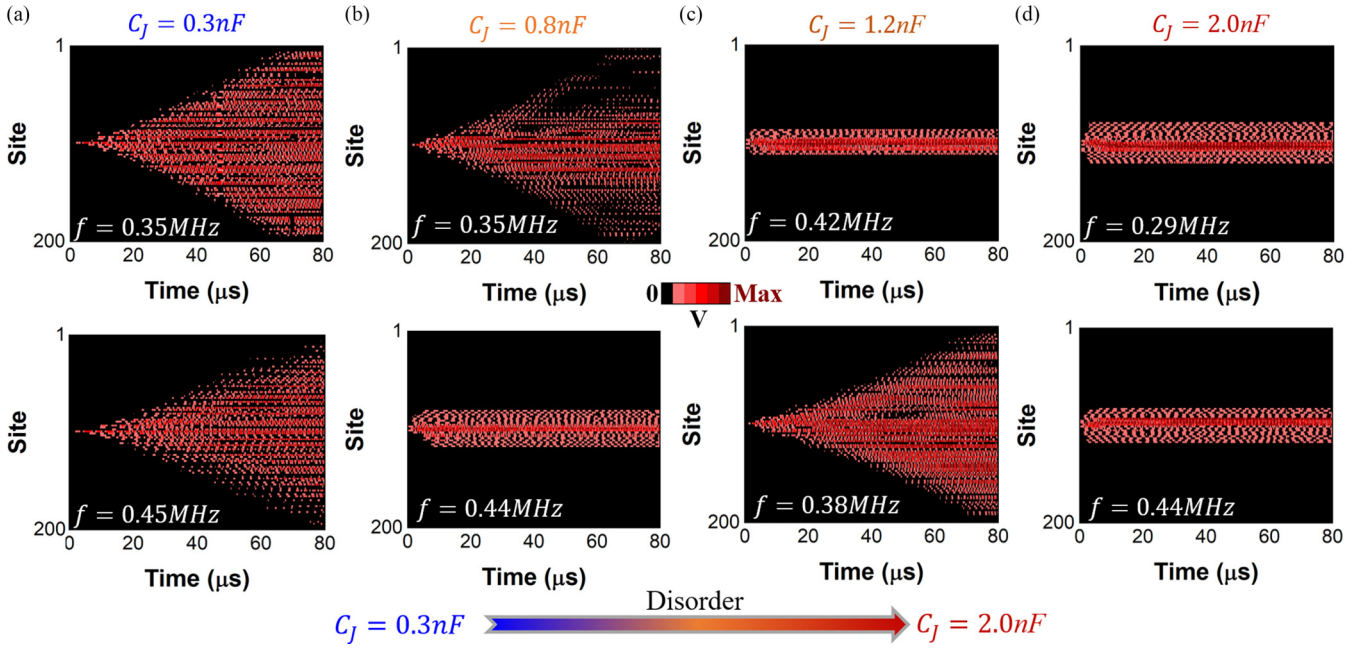
FIG. 4. Observation of non-Abelian Anderson localization and transition by the temporal dynamics in one-dimensional (1D) non-Abelian Aubry-André-Harper (AAH) circuits. (a)–(d) Experiment results of voltage dynamics at two circuit nodes in the 1D non-Abelian AAH circuits staying in the delocalization phase with $C_J = 0.3nF$, the coexistence phase I with $C_J = 0.8nF$, the coexistence phase II with $C_J = 1.2nF$, and the localization phase with $C_J = 2nF$. Here, the circuit excitation is in the form of $[V_{1,50_\uparrow} = V_0 e^{i\omega t}, V_{2,50_\uparrow} = -V_0 e^{i\omega t}]$ being consistent with the eigenmode of $|\uparrow\rangle$ at the 50th lattice site. The excitation frequency is shown in each subplot.

IV. CONCLUSIONS

In conclusion, we have experimentally investigated non-Abelian Anderson localization and transition in 1D non-Abelian AAH electrical circuits with different disorder strengths, where the eigenmodes of the non-Abelian AAH model are mapped to the designed electrical circuit simulators. Based on the flexibly of circuit connections and groundings, different strengths of disorder can be suitably introduced into the 1D effective non-Abelian AAH circuit. In this case, through the direct measurements of site-resolved impedance spectra and time-domain voltage dynamics, different types of non-Abelian Anderson phases, including the delocalization phase, coexisting states with localized and delocalized spatial profiles, and the localization phase can be clearly observed. In addition, the investigation of interplays between non-Abelian gauge potential and Anderson localization can be further extended into non-Hermitian, nonlinear, and high-dimensional systems, which can also be implemented in electrical circuits. Our proposal provides a flexible platform to investigate Anderson localization driven by non-Abelian gauge potentials and could

have potential applications in the field of the electrical signal control.

APPENDIX A: DETAILS FOR DERIVATION OF THE EIGENEQUATION FOR THE 1D NON-ABELIAN CIRCUIT SIMULATOR

In this appendix, we give a detailed derivation of the circuit eigenequation, which could be mapped to the 1D stationary Schrödinger equation of the non-Abelian AAH model. Here, each lattice site contains two pairs of circuit nodes. In this case, the voltage and current at site n should be written as $V_n = [V_{1,n_\sigma}, V_{2,n_\sigma}]^T$ and $I = [I_{1,n_\sigma}, I_{2,n_\sigma}]^T$ ($\sigma = |\uparrow\rangle, |\downarrow\rangle$). The voltages on the circuit nodes are in the form of $V_{1,n_\sigma} e^{j\omega t}$ and $V_{2,n_\sigma} e^{j\omega t}$. Carrying out the Kirchhoff's law on the circuit node pair n_σ, we get the following equations:

$$
\begin{vmatrix} I_{1,n_\uparrow} \\ I_{2,n_\uparrow} \\ I_{1,n_\downarrow} \\ I_{2,n_\downarrow} \end{vmatrix} = i\omega^{-1} \left\{ \omega^2 C \begin{bmatrix} 1 & -1 & 0 & 0 \\ -1 & 1 & 0 & 0 \\ 0 & 0 & 1 & -1 \\ 0 & 0 & -1 & 1 \end{bmatrix} \begin{vmatrix} V_{1,n_\uparrow} \\ V_{2,n_\uparrow} \\ V_{1,n_\downarrow} \\ V_{2,n_\downarrow} \end{vmatrix} + \omega^2 C_c \begin{vmatrix} V_{1,n_\uparrow} - V_{1,n+1_\uparrow} \\ V_{2,n_\uparrow} - V_{2,n+1_\uparrow} \\ V_{1,n_\downarrow} - V_{1,n+1_\downarrow} \\ V_{2,n_\downarrow} - V_{2,n+1_\downarrow} \end{vmatrix} + \omega^2 C_s \begin{vmatrix} V_{1,n_\uparrow} - V_{1,n+1_\downarrow} \\ V_{2,n_\uparrow} - V_{2,n+1_\downarrow} \\ V_{1,n_\downarrow} - V_{2,n+1_\uparrow} \\ V_{2,n_\downarrow} - V_{1,n+1_\uparrow} \end{vmatrix} \right.
$$

$$
+ \omega^2 C_c \begin{vmatrix} V_{1,n_\uparrow} - V_{1,n-1_\uparrow} \\ V_{2,n_\uparrow} - V_{2,n-1_\uparrow} \\ V_{1,n_\downarrow} - V_{1,n-1_\downarrow} \\ V_{2,n_\downarrow} - V_{2,n-1_\downarrow} \end{vmatrix} + \omega^2 C_s \begin{vmatrix} V_{1,n_\uparrow} - V_{2,n-1_\downarrow} \\ V_{2,n_\uparrow} - V_{1,n-1_\downarrow} \\ V_{1,n_\downarrow} - V_{1,n-1_\uparrow} \\ V_{2,n_\downarrow} - V_{2,n-1_\uparrow} \end{vmatrix} + \omega^2 C_n \begin{vmatrix} V_{1,n_\uparrow} \\ V_{2,n_\uparrow} \\ V_{1,n_\downarrow} \\ V_{2,n_\downarrow} \end{vmatrix} + \omega^2 C_{n'} \begin{vmatrix} V_{1,n_\uparrow} - V_{1,n_\downarrow} \\ V_{2,n_\uparrow} - V_{2,n_\downarrow} \\ V_{1,n_\downarrow} - V_{1,n_\uparrow} \\ V_{2,n_\downarrow} - V_{2,n_\uparrow} \end{vmatrix} + \omega^2 C_u \begin{vmatrix} V_{1,n_\uparrow} \\ V_{2,n_\uparrow} \\ V_{1,n_\downarrow} \\ V_{2,n_\downarrow} \end{vmatrix} - \frac{1}{L_g} \begin{vmatrix} V_{1,n_\uparrow} \\ V_{2,n_\uparrow} \\ V_{1,n_\downarrow} \\ V_{2,n_\downarrow} \end{vmatrix} \Bigg\},
\tag{A1}
$$

$$
\begin{vmatrix} I_{1,n_\uparrow} \\ I_{2,n_\uparrow} \\ I_{1,n_\downarrow} \\ I_{2,n_\downarrow} \end{vmatrix} = i\omega^{-1} \Bigg\{ \omega^2 C \begin{bmatrix} 1 & -1 & 0 & 0 \\ -1 & 1 & 0 & 0 \\ 0 & 0 & 1 & -1 \\ 0 & 0 & -1 & 1 \end{bmatrix} \begin{vmatrix} V_{1,n_\uparrow} \\ V_{2,n_\uparrow} \\ V_{1,n_\downarrow} \\ V_{2,n_\downarrow} \end{vmatrix} + \omega^2 C_c \begin{vmatrix} V_{1,n_\uparrow} - V_{1,n+1_\uparrow} \\ V_{2,n_\uparrow} - V_{2,n+1_\uparrow} \\ V_{1,n_\downarrow} - V_{1,n+1_\downarrow} \\ V_{2,n_\downarrow} - V_{2,n+1_\downarrow} \end{vmatrix}
$$

$$
+ \omega^2 C_s \begin{vmatrix} V_{1,n_\uparrow} - V_{1,n+1_\downarrow} \\ V_{2,n_\uparrow} - V_{2,n+1_\downarrow} \\ V_{1,n_\downarrow} - V_{2,n+1_\uparrow} \\ V_{2,n_\downarrow} - V_{1,n+1_\uparrow} \end{vmatrix} + \omega^2 C_c \begin{vmatrix} V_{1,n_\uparrow} - V_{1,n-1_\uparrow} \\ V_{2,n_\uparrow} - V_{2,n-1_\uparrow} \\ V_{1,n_\downarrow} - V_{1,n-1_\downarrow} \\ V_{2,n_\downarrow} - V_{2,n-1_\downarrow} \end{vmatrix} + \omega^2 C_s \begin{vmatrix} V_{1,n_\uparrow} - V_{2,n-1_\downarrow} \\ V_{2,n_\uparrow} - V_{1,n-1_\downarrow} \\ V_{1,n_\downarrow} - V_{1,n-1_\uparrow} \\ V_{2,n_\downarrow} - V_{2,n-1_\uparrow} \end{vmatrix} + \omega^2 C_n \begin{vmatrix} V_{1,n_\uparrow} \\ V_{2,n_\uparrow} \\ V_{1,n_\downarrow} \\ V_{2,n_\downarrow} \end{vmatrix}
$$

$$
+ \omega^2 C_{n'} \begin{vmatrix} V_{1,n_\uparrow} - V_{2,n_\downarrow} \\ V_{2,n_\uparrow} - V_{1,n_\downarrow} \\ V_{1,n_\downarrow} - V_{2,n_\uparrow} \\ V_{2,n_\downarrow} - V_{1,n_\uparrow} \end{vmatrix} + \omega^2 C_u \begin{vmatrix} V_{1,n_\uparrow} \\ V_{2,n_\uparrow} \\ V_{1,n_\downarrow} \\ V_{2,n_\downarrow} \end{vmatrix} - \frac{1}{L_g} \begin{vmatrix} V_{1,n_\uparrow} \\ V_{2,n_\uparrow} \\ V_{1,n_\downarrow} \\ V_{2,n_\downarrow} \end{vmatrix} \Bigg\}.
\tag{A2}
$$

It is worth noting that Eqs. (A1) and (A2) correspond to cases with two node pairs at the nth site being connected without and with a cross, respectively. Here, L_g is the grounding inductor, C is the capacitance used to link two circuit nodes to form an internal degree at each lattice site, C_c and C_s are capacitances for connecting circuit node pairs with (without) a cross, indicating the negative (positive) intersite coupling, and C_u is an extra grounding capacitor to ensure a positive value of the sum for all grounding capacitors. In addition, capacitors C_n and $C_{n'}$ create the diagonal and nondiagonal elements of the modulation matrix U_n. We assume that there is no external source, so that the current flowing out of the node is zero. In this case, Eqs. (A1) and (A2) become

$$
-\omega^2 C \begin{bmatrix} 1 & -1 & 0 & 0 \\ -1 & 1 & 0 & 0 \\ 0 & 0 & 1 & -1 \\ 0 & 0 & -1 & 1 \end{bmatrix} \begin{vmatrix} V_{1,n_\uparrow} \\ V_{2,n_\uparrow} \\ V_{1,n_\downarrow} \\ V_{2,n_\downarrow} \end{vmatrix} = \omega^2 (2C_c + 2C_s + C_{n'}) \begin{vmatrix} V_{1,n_\uparrow} \\ V_{2,n_\uparrow} \\ V_{1,n_\downarrow} \\ V_{2,n_\downarrow} \end{vmatrix} - \omega^2 C_c \begin{vmatrix} V_{1,n+1_\uparrow} \\ V_{2,n+1_\uparrow} \\ V_{1,n+1_\downarrow} \\ V_{2,n+1_\downarrow} \end{vmatrix} - \omega^2 C_s \begin{bmatrix} 1 & 0 & 0 & 0 \\ 0 & 1 & 0 & 0 \\ 0 & 0 & 0 & 1 \\ 0 & 0 & 1 & 0 \end{bmatrix} \begin{vmatrix} V_{1,n+1_\downarrow} \\ V_{2,n+1_\downarrow} \\ V_{1,n+1_\uparrow} \\ V_{2,n+1_\uparrow} \end{vmatrix}
$$

$$
- \omega^2 C_c \begin{vmatrix} V_{1,n-1_\uparrow} \\ V_{2,n-1_\uparrow} \\ V_{1,n-1_\downarrow} \\ V_{2,n-1_\downarrow} \end{vmatrix} - \omega^2 C_s \begin{bmatrix} 0 & 1 & 0 & 0 \\ 1 & 0 & 0 & 0 \\ 0 & 0 & 1 & 0 \\ 0 & 0 & 0 & 1 \end{bmatrix} \begin{vmatrix} V_{1,n-1_\downarrow} \\ V_{2,n-1_\downarrow} \\ V_{1,n-1_\uparrow} \\ V_{2,n-1_\uparrow} \end{vmatrix} + \omega^2 C_n \begin{vmatrix} V_{1,n_\uparrow} \\ V_{2,n_\uparrow} \\ V_{1,n_\downarrow} \\ V_{2,n_\downarrow} \end{vmatrix}
$$

$$
- \omega^2 C_{n'} \begin{bmatrix} 1 & 0 & 0 & 0 \\ 0 & 1 & 0 & 0 \\ 0 & 0 & 1 & 0 \\ 0 & 0 & 0 & 1 \end{bmatrix} \begin{vmatrix} V_{1,n_\downarrow} \\ V_{2,n_\downarrow} \\ V_{1,n_\uparrow} \\ V_{2,n_\uparrow} \end{vmatrix} + \omega^2 C_u \begin{vmatrix} V_{1,n_\uparrow} \\ V_{2,n_\uparrow} \\ V_{1,n_\downarrow} \\ V_{2,n_\downarrow} \end{vmatrix} - \frac{1}{L_g} \begin{vmatrix} V_{1,n_\uparrow} \\ V_{2,n_\uparrow} \\ V_{1,n_\downarrow} \\ V_{2,n_\downarrow} \end{vmatrix},
\tag{A3}
$$

$$
-\omega^2 C \begin{bmatrix} 1 & -1 & 0 & 0 \\ -1 & 1 & 0 & 0 \\ 0 & 0 & 1 & -1 \\ 0 & 0 & -1 & 1 \end{bmatrix} \begin{vmatrix} V_{1,n_\uparrow} \\ V_{2,n_\uparrow} \\ V_{1,n_\downarrow} \\ V_{2,n_\downarrow} \end{vmatrix} = \omega^2 (2C_c + 2C_s + C_{n'}) \begin{vmatrix} V_{1,n_\uparrow} \\ V_{2,n_\uparrow} \\ V_{1,n_\downarrow} \\ V_{2,n_\downarrow} \end{vmatrix} - \omega^2 C_c \begin{vmatrix} V_{1,n+1_\uparrow} \\ V_{2,n+1_\uparrow} \\ V_{1,n+1_\downarrow} \\ V_{2,n+1_\downarrow} \end{vmatrix} - \omega^2 C_s \begin{bmatrix} 1 & 0 & 0 & 0 \\ 0 & 1 & 0 & 0 \\ 0 & 0 & 0 & 1 \\ 0 & 0 & 1 & 0 \end{bmatrix} \begin{vmatrix} V_{1,n+1_\downarrow} \\ V_{2,n+1_\downarrow} \\ V_{1,n+1_\uparrow} \\ V_{2,n+1_\uparrow} \end{vmatrix}
$$

$$
- \omega^2 C_c \begin{vmatrix} V_{1,n-1_\uparrow} \\ V_{2,n-1_\uparrow} \\ V_{1,n-1_\downarrow} \\ V_{2,n-1_\downarrow} \end{vmatrix} - \omega^2 C_s \begin{bmatrix} 0 & 1 & 0 & 0 \\ 1 & 0 & 0 & 0 \\ 0 & 0 & 1 & 0 \\ 0 & 0 & 0 & 1 \end{bmatrix} \begin{vmatrix} V_{1,n-1_\downarrow} \\ V_{2,n-1_\downarrow} \\ V_{1,n-1_\uparrow} \\ V_{2,n-1_\uparrow} \end{vmatrix} + \omega^2 C_n \begin{vmatrix} V_{1,n_\uparrow} \\ V_{2,n_\uparrow} \\ V_{1,n_\downarrow} \\ V_{2,n_\downarrow} \end{vmatrix}
$$

$$
- \omega^2 C_{n'} \begin{bmatrix} 0 & 1 & 0 & 0 \\ 1 & 0 & 0 & 0 \\ 0 & 0 & 0 & 1 \\ 0 & 0 & 1 & 0 \end{bmatrix} \begin{vmatrix} V_{1,n_\downarrow} \\ V_{2,n_\downarrow} \\ V_{1,n_\uparrow} \\ V_{2,n_\uparrow} \end{vmatrix} + \omega^2 C_u \begin{vmatrix} V_{1,n_\uparrow} \\ V_{2,n_\uparrow} \\ V_{1,n_\downarrow} \\ V_{2,n_\downarrow} \end{vmatrix} - \frac{1}{L_g} \begin{vmatrix} V_{1,n_\uparrow} \\ V_{2,n_\uparrow} \\ V_{1,n_\downarrow} \\ V_{2,n_\downarrow} \end{vmatrix}.
\tag{A4}
$$

Performing the diagonalization of Eqs. (A3) and (A4) with a unitary transformation:

$$
F = \mathrm{diag}(U, U), \quad \text{with} \quad U = \frac{1}{\sqrt{2}} \begin{bmatrix} 1 & 1 \\ 1 & -1 \end{bmatrix},
\tag{A5}
$$

Eqs. (A3) and (A4) become

$$
-C\begin{bmatrix}0&0&0&0\\0&2&0&0\\0&0&0&0\\0&0&0&2\end{bmatrix}\begin{vmatrix}V_{S,n_\uparrow}\\V_{A,n_\uparrow}\\V_{S,n_\downarrow}\\V_{A,n_\downarrow}\end{vmatrix}=(2C_c+2C_s+C_{n'})\begin{vmatrix}V_{S,n_\uparrow}\\V_{A,n_\uparrow}\\V_{S,n_\downarrow}\\V_{A,n_\downarrow}\end{vmatrix}-C_c\begin{vmatrix}V_{S,n+1_\uparrow}\\V_{A,n+1_\uparrow}\\V_{S,n+1_\downarrow}\\V_{A,n+1_\downarrow}\end{vmatrix}-C_s\begin{bmatrix}1&0&0&0\\0&1&0&0\\0&0&1&0\\0&0&0&-1\end{bmatrix}\begin{vmatrix}V_{S,n+1_\downarrow}\\V_{A,n+1_\downarrow}\\V_{S,n+1_\uparrow}\\V_{A,n+1_\uparrow}\end{vmatrix}
$$

$$
-C_c\begin{vmatrix}V_{S,n-1_\uparrow}\\V_{A,n-1_\uparrow}\\V_{S,n-1_\downarrow}\\V_{A,n-1_\downarrow}\end{vmatrix}-C_s\begin{bmatrix}1&0&0&0\\0&-1&0&0\\0&0&1&0\\0&0&0&1\end{bmatrix}\begin{vmatrix}V_{S,n-1_\downarrow}\\V_{A,n-1_\downarrow}\\V_{S,n-1_\uparrow}\\V_{A,n-1_\uparrow}\end{vmatrix}+C_n\begin{vmatrix}V_{S,n_\uparrow}\\V_{A,n_\uparrow}\\V_{S,n_\downarrow}\\V_{A,n_\downarrow}\end{vmatrix}
$$

$$
-C_{n'}\begin{bmatrix}1&0&0&0\\0&1&0&0\\0&0&1&0\\0&0&0&1\end{bmatrix}\begin{vmatrix}V_{S,n_\downarrow}\\V_{A,n_\downarrow}\\V_{S,n_\uparrow}\\V_{A,n_\uparrow}\end{vmatrix}+C_u\begin{vmatrix}V_{S,n_\uparrow}\\V_{A,n_\uparrow}\\V_{S,n_\downarrow}\\V_{A,n_\downarrow}\end{vmatrix}-\frac{1}{\omega^2 L_g}\begin{vmatrix}V_{S,n_\uparrow}\\V_{A,n_\uparrow}\\V_{S,n_\downarrow}\\V_{A,n_\downarrow}\end{vmatrix},\tag{A6}
$$

$$
-C\begin{bmatrix}0&0&0&0\\0&2&0&0\\0&0&0&0\\0&0&0&2\end{bmatrix}\begin{vmatrix}V_{S,n_\uparrow}\\V_{A,n_\uparrow}\\V_{S,n_\downarrow}\\V_{A,n_\downarrow}\end{vmatrix}=(2C_c+2C_s+C_{n'})\begin{vmatrix}V_{S,n_\uparrow}\\V_{A,n_\uparrow}\\V_{S,n_\downarrow}\\V_{A,n_\downarrow}\end{vmatrix}-C_c\begin{vmatrix}V_{S,n+1_\uparrow}\\V_{A,n+1_\uparrow}\\V_{S,n+1_\downarrow}\\V_{A,n+1_\downarrow}\end{vmatrix}-C_s\begin{bmatrix}1&0&0&0\\0&1&0&0\\0&0&1&0\\0&0&0&-1\end{bmatrix}\begin{vmatrix}V_{S,n+1_\downarrow}\\V_{A,n+1_\downarrow}\\V_{S,n+1_\uparrow}\\V_{A,n+1_\uparrow}\end{vmatrix}
$$

$$
-C_c\begin{vmatrix}V_{S,n-1_\uparrow}\\V_{A,n-1_\uparrow}\\V_{S,n-1_\downarrow}\\V_{A,n-1_\downarrow}\end{vmatrix}-C_s\begin{bmatrix}1&0&0&0\\0&-1&0&0\\0&0&1&0\\0&0&0&1\end{bmatrix}\begin{vmatrix}V_{S,n-1_\downarrow}\\V_{A,n-1_\downarrow}\\V_{S,n-1_\uparrow}\\V_{A,n-1_\uparrow}\end{vmatrix}+C_n\begin{vmatrix}V_{S,n_\uparrow}\\V_{A,n_\uparrow}\\V_{S,n_\downarrow}\\V_{A,n_\downarrow}\end{vmatrix}
$$

$$
-C_{n'}\begin{bmatrix}1&0&0&0\\0&-1&0&0\\0&0&1&0\\0&0&0&-1\end{bmatrix}\begin{vmatrix}V_{S,n_\downarrow}\\V_{A,n_\downarrow}\\V_{S,n_\uparrow}\\V_{A,n_\uparrow}\end{vmatrix}+C_u\begin{vmatrix}V_{S,n_\uparrow}\\V_{A,n_\uparrow}\\V_{S,n_\downarrow}\\V_{A,n_\downarrow}\end{vmatrix}-\frac{1}{\omega^2 L_g}\begin{vmatrix}V_{S,n_\uparrow}\\V_{A,n_\uparrow}\\V_{S,n_\downarrow}\\V_{A,n_\downarrow}\end{vmatrix}.\tag{A7}
$$

The new basis can be expressed as $[V_{S,n_\sigma},V_{A,n_\sigma}]^T=U[V_{n_\sigma,1},V_{n_\sigma,2}]^T$, with $V_{S,n_\sigma}=(V_{1,n_\sigma}+V_{2,n_\sigma})/\sqrt{2}$ and $V_{A,n_\sigma}=(V_{1,n_\sigma}-V_{2,n_\sigma})/\sqrt{2}$ ($\sigma=|\uparrow\rangle,|\downarrow\rangle$), which create two decoupled subspaces. Thus, both Eqs. (A6) and (A7) can be divided into two independent equations as

$$
\frac{1}{\omega^2 L_g C}\begin{vmatrix}V_{S,n_\uparrow}\\V_{S,n_\downarrow}\end{vmatrix}=\left(2\frac{C_c}{C}+2\frac{C_s}{C}+\frac{C_{n'}}{C}\right)\begin{vmatrix}V_{S,n_\uparrow}\\V_{S,n_\downarrow}\end{vmatrix}-\frac{C_c}{C}\left(\begin{vmatrix}V_{S,n+1_\uparrow}\\V_{S,n+1_\downarrow}\end{vmatrix}+\begin{vmatrix}V_{S,n-1_\uparrow}\\V_{S,n-1_\downarrow}\end{vmatrix}\right)-\frac{C_s}{C}\left(\begin{bmatrix}0&1\\1&0\end{bmatrix}\begin{vmatrix}V_{S,n+1_\uparrow}\\V_{S,n+1_\downarrow}\end{vmatrix}\right.
$$

$$
\left.+\begin{bmatrix}0&1\\1&0\end{bmatrix}\begin{vmatrix}V_{S,n-1_\uparrow}\\V_{S,n-1_\downarrow}\end{vmatrix}\right)+\frac{C_n}{C}\begin{vmatrix}V_{S,n_\uparrow}\\V_{S,n_\downarrow}\end{vmatrix}-\frac{C_{n'}}{C}\begin{bmatrix}0&1\\1&0\end{bmatrix}\begin{vmatrix}V_{S,n_\uparrow}\\V_{S,n_\downarrow}\end{vmatrix}+\frac{C_u}{C}\begin{vmatrix}V_{S,n_\uparrow}\\V_{S,n_\downarrow}\end{vmatrix},
$$

$$
\left(\frac{1}{\omega^2 L_g C}-2\right)\begin{vmatrix}V_{A,n_\uparrow}\\V_{A,n_\downarrow}\end{vmatrix}=\left(2\frac{C_c}{C}+2\frac{C_s}{C}+\frac{C_{n'}}{C}\right)\begin{vmatrix}V_{A,n_\uparrow}\\V_{A,n_\downarrow}\end{vmatrix}-\frac{C_c}{C}\left(\begin{vmatrix}V_{A,n+1_\uparrow}\\V_{A,n+1_\downarrow}\end{vmatrix}+\begin{vmatrix}V_{A,n-1_\uparrow}\\V_{A,n-1_\downarrow}\end{vmatrix}\right)
$$

$$
-\frac{C_s}{C}\left(\begin{bmatrix}0&1\\-1&0\end{bmatrix}\begin{vmatrix}V_{A,n+1_\uparrow}\\V_{A,n+1_\downarrow}\end{vmatrix}+\begin{bmatrix}0&-1\\1&0\end{bmatrix}\begin{vmatrix}V_{A,n-1_\uparrow}\\V_{A,n-1_\downarrow}\end{vmatrix}\right)+\frac{C_n}{C}\begin{vmatrix}V_{A,n_\uparrow}\\V_{A,n_\downarrow}\end{vmatrix}-\frac{C_{n'}}{C}\begin{bmatrix}0&1\\1&0\end{bmatrix}\begin{vmatrix}V_{A,n_\uparrow}\\V_{A,n_\downarrow}\end{vmatrix}+\frac{C_u}{C}\begin{vmatrix}V_{A,n_\uparrow}\\V_{A,n_\downarrow}\end{vmatrix},
$$
$$\tag{A8}$$

$$
\frac{1}{\omega^2 L_g C}\begin{vmatrix}V_{S,n_\uparrow}\\V_{S,n_\downarrow}\end{vmatrix}=\left(2\frac{C_c}{C}+2\frac{C_s}{C}+\frac{C_{n'}}{C}\right)\begin{vmatrix}V_{S,n_\uparrow}\\V_{S,n_\downarrow}\end{vmatrix}-\frac{C_c}{C}\left(\begin{vmatrix}V_{S,n+1_\uparrow}\\V_{S,n+1_\downarrow}\end{vmatrix}+\begin{vmatrix}V_{S,n-1_\uparrow}\\V_{S,n-1_\downarrow}\end{vmatrix}\right)-\frac{C_s}{C}\left(\begin{bmatrix}0&1\\1&0\end{bmatrix}\begin{vmatrix}V_{S,n+1_\uparrow}\\V_{S,n+1_\downarrow}\end{vmatrix}\right.
$$

$$
\left.+\begin{bmatrix}0&1\\1&0\end{bmatrix}\begin{vmatrix}V_{S,n-1_\uparrow}\\V_{S,n-1_\downarrow}\end{vmatrix}\right)+\frac{C_n}{C}\begin{vmatrix}V_{S,n_\uparrow}\\V_{S,n_\downarrow}\end{vmatrix}-\frac{C_{n'}}{C}\begin{bmatrix}0&1\\1&0\end{bmatrix}\begin{vmatrix}V_{S,n_\uparrow}\\V_{S,n_\downarrow}\end{vmatrix}+\frac{C_u}{C}\begin{vmatrix}V_{S,n_\uparrow}\\V_{S,n_\downarrow}\end{vmatrix},
$$

$$
\left(\frac{1}{\omega^2 L_g C}-2\right)\begin{vmatrix}V_{A,n_\uparrow}\\V_{A,n_\downarrow}\end{vmatrix}=\left(2\frac{C_c}{C}+2\frac{C_s}{C}+\frac{C_{n'}}{C}\right)\begin{vmatrix}V_{A,n_\uparrow}\\V_{A,n_\downarrow}\end{vmatrix}-\frac{C_c}{C}\left(\begin{vmatrix}V_{A,n+1_\uparrow}\\V_{A,n+1_\downarrow}\end{vmatrix}+\begin{vmatrix}V_{A,n-1_\uparrow}\\V_{A,n-1_\downarrow}\end{vmatrix}\right)
$$

$$
-\frac{C_s}{C}\left(\begin{bmatrix}0&1\\-1&0\end{bmatrix}\begin{vmatrix}V_{A,n+1_\uparrow}\\V_{A,n+1_\downarrow}\end{vmatrix}+\begin{bmatrix}0&-1\\1&0\end{bmatrix}\begin{vmatrix}V_{A,n-1_\uparrow}\\V_{A,n-1_\downarrow}\end{vmatrix}\right)+\frac{C_n}{C}\begin{vmatrix}V_{A,n_\uparrow}\\V_{A,n_\downarrow}\end{vmatrix}-\frac{C_{n'}}{C}\begin{bmatrix}0&-1\\-1&0\end{bmatrix}\begin{vmatrix}V_{A,n_\uparrow}\\V_{A,n_\downarrow}\end{vmatrix}+\frac{C_u}{C}\begin{vmatrix}V_{A,n_\uparrow}\\V_{A,n_\downarrow}\end{vmatrix}.
$$
$$\tag{A9}$$

Combing the second formula of Eqs. (A8) and (A9) for V_{A,n_σ}, the eigenequation of the designed non-Abelian electrical circuit is described by

$$
\left(\frac{f_0^2}{f^2} - 2 - 2\frac{C_c}{C} - 2\frac{C_s}{C} - \frac{C_u}{C} - \frac{C_{n'}}{C} \right) \begin{vmatrix} V_{A,n_\uparrow} \\ V_{A,n_\downarrow} \end{vmatrix} = - \begin{bmatrix} \frac{C_c}{C} & \frac{C_s}{C} \\ -\frac{C_s}{C} & \frac{C_c}{C} \end{bmatrix} \begin{vmatrix} V_{A,n+1_\uparrow} \\ V_{A,n+1_\downarrow} \end{vmatrix} - \begin{bmatrix} \frac{C_c}{C} & -\frac{C_s}{C} \\ \frac{C_s}{C} & \frac{C_c}{C} \end{bmatrix} \begin{vmatrix} V_{A,n-1_\uparrow} \\ V_{A,n-1_\downarrow} \end{vmatrix} + \begin{bmatrix} \frac{C_n}{C} & -\frac{C_{n'}}{C} \\ -\frac{C_{n'}}{C} & \frac{C_n}{C} \end{bmatrix} \begin{vmatrix} V_{A,n_\uparrow} \\ V_{A,n_\downarrow} \end{vmatrix}.
$$
(A10)

We provide the following identification of tight-binding parameters in terms of circuit elements as

$$
U = \frac{C_u}{C}, \quad \cos q = \frac{C_c}{C}, \quad \sin q = \frac{C_s}{C}, \quad \frac{C_n}{C} = 2J\cos(q)\cos(2\pi\chi n), \quad \frac{C_{n'}}{C} = 2J\sin(q)\sin(2\pi\chi n),
$$

$$
\varepsilon = \left(\frac{f_0^2}{f^2} - 2 - 2\frac{C_c}{C} - 2\frac{C_s}{C} - \frac{C_u}{C} - \frac{C_{n'}}{C} \right), \quad f_0 = \frac{1}{2\pi\sqrt{L_g C}},
$$

$$
M = \begin{pmatrix} \cos q & \sin q \\ -\sin q & \cos q \end{pmatrix}, \quad U_n = 2J \begin{bmatrix} \cos q \cos(2\pi\chi n) & -\sin q \sin(2\pi\chi n) \\ -\sin q \sin(2\pi\chi n) & \cos q \cos(2\pi\chi n) \end{bmatrix},
$$

where ε corresponds to the eigenenergy, and M and U_n are the coupling and on-site modulation matrixes, respectively. In this case, Eq (A10) becomes

$$
\varepsilon \begin{pmatrix} \varphi_{\psi_{n,\uparrow}} \\ \varphi_{\psi_{n,\downarrow}} \end{pmatrix} = M \begin{pmatrix} \varphi_{\psi_{n+1,\uparrow}} \\ \varphi_{\psi_{n+1,\downarrow}} \end{pmatrix} + M^+ \begin{pmatrix} \varphi_{\psi_{n-1,\uparrow}} \\ \varphi_{\psi_{n-1,\downarrow}} \end{pmatrix} + U_n \begin{pmatrix} \varphi_{\psi_{n,\uparrow}} \\ \varphi_{\psi_{n,\downarrow}} \end{pmatrix},
$$
(A11)

with $\varphi_{\psi_{n,\uparrow}}$ and $\varphi_{\psi_{n,\downarrow}}$ corresponding to $V_{A,n_\uparrow}$ and $V_{A,n_\downarrow}$. In this case, we can see that the circuit eigenequation is identical to the 1D non-Abelian AAH model. In addition, the derived eigenequation of the symmetric sector V_S is expressed as

$$
\left(\frac{f_0^2}{f^2} - 2\frac{C_c}{C} - 2\frac{C_s}{C} - \frac{C_u}{C} - \frac{C_{n'}}{C} \right) \begin{vmatrix} V_{s,n_\uparrow} \\ V_{s,n_\downarrow} \end{vmatrix} = - \begin{bmatrix} \frac{C_c}{C} & \frac{C_s}{C} \\ \frac{C_s}{C} & \frac{C_c}{C} \end{bmatrix} \begin{vmatrix} V_{S,n+1_\uparrow} \\ V_{S,n+1_\downarrow} \end{vmatrix} - \begin{bmatrix} \frac{C_c}{C} & \frac{C_s}{C} \\ \frac{C_s}{C} & \frac{C_c}{C} \end{bmatrix} \begin{vmatrix} V_{S,n-1_\uparrow} \\ V_{S,n-1_\downarrow} \end{vmatrix} + \begin{bmatrix} \frac{C_n}{C} & -\frac{C_{n'}}{C} \\ -\frac{C_{n'}}{C} & \frac{C_n}{C} \end{bmatrix} \begin{vmatrix} V_{S,n_\uparrow} \\ V_{S,n_\downarrow} \end{vmatrix},
$$
(A12)

where the coupling matrix is different from that of the non-Abelian AAH model. The energy spectrum of the symmetric sector V_S is given by $\varepsilon = \frac{f_0^2}{f^2} - 2\frac{C_c}{C} - 2\frac{C_s}{C} - \frac{C_u}{C} - \frac{C_{n'}}{C}$, which differs from the on-site term in the V_{A,n_σ} sector, resulting in a downward shift of the eigenenergy of the V_{S,n_σ} sector relative to that of V_{A,n_σ}.

APPENDIX B: SAMPLE FABRICATIONS AND CIRCUIT MEASUREMENTS

We exploit the non-Abelian AAH circuits by using PADs program software. Here, the well-designed printed circuit board (PCB) possesses totally four layers to arrange non-Abelian coupling matrices and on-site potentials. The grounding layer should be placed in the gap between the other two layers. Moreover, all PCB traces have relatively large widths (0.5 mm) to reduce the parasitic inductance, and distances between electronic devices are also >1.0 mm to avert spurious inductive coupling. Sub miniature push-on (SMP) connectors are welded on PCB nodes for the signal input and detection. In addition, we use a WK6500B impedance analyzer to select circuit elements with high accuracy (the disorder strength is only 1%) and low losses. Figure 3 presents the front and back sides of photograph images for the fabricated non-Abelian AAH circuits with different strengths of disorder.

As for the measurement of the voltage evolution in the time domain, we use the signal generator (NI PXI-5404) with eight output ports to act as the current source for exciting two circuit nodes related to a single lattice site with constant amplitude and node-dependent initial phases. We measure the voltage

signal at one circuit node. The generator (the initial phase is set to 0) is directly connected to one end of the oscilloscope (Agilent Technologies Infiniivision DSO7104B) to ensure an accurate start time. The measured voltage signals are in the range from 0 to 5 ms, where 0 ms is defined as the time for the simultaneously signal injection and measurement.

APPENDIX C: IMPEDANCE SPECTRA IN THE PSEUDOSPIN SUBSPACE OF $|\downarrow\rangle$

Here, we present the measured impedance responses in the pseudospin subspace of $|\downarrow\rangle$. The blue and orange lines in Fig. 5 present the experiment results of two typical circuit nodes ($n = 24$ and 70) with different strengths of disorder ($C_J = 0.3nF$, $0.8nF$, $1.2nF$, and $2.0nF$). Figure 5(a) gives impedance responses of two different circuit nodes with $C_J = 0.3nF$, which belongs to the delocalization phase. It is shown that there are many impedance peaks with small values at different frequencies ranging from 0.25 to 0.55 MHz of these two circuit nodes. These results clearly indicate the extension of the eigenspectrum as well as the delocalization of the corresponding eigenfields. Then we measure the impedance spectra with $C_J = 0.8nF$ at these two nodes, as shown in Fig. 5(b). We can see that the measurement results at different circuit nodes are completely opposite. It is found that a large-valued impedance peak (the blue line with $n = 24$) is located at 0.44 MHz. On the contrary, there are many impedance peaks with small values (the orange line) when the other circuit node ($n = 70$) is excited. These results show the coexistence of delocalized and localized eigenstates at $C_J = 0.8nF$, which correspond to the feature of coexistence phase I. Furthermore,
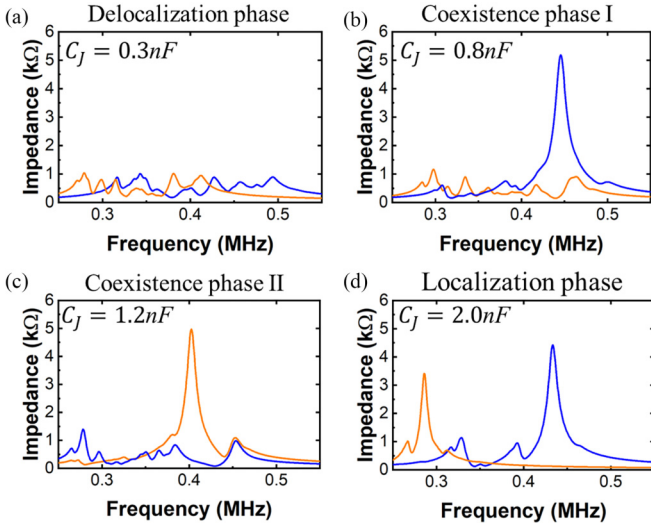
FIG. 5. Experimental impedance spectra in the pseudospin subspace of $|\downarrow\rangle$. (a) Measured impedance responses with $C_J = 0.3nF$, which correspond to the delocalization phase. (b) and (c) Measured impedance spectra of coexistence phases I and II in designed one-dimensional (1D) non-Abelian Aubry-André-Harper (AAH) circuits with disorder strengths set as $C_J = 0.8nF$ and $1.2nF$, respectively. (d) Measured impedance responses with $C_J = 2.0nF$, corresponding to the localization phase of the non-Abelian AAH circuit. The blue and orange lines represent impedance spectra at two different circuit nodes of $n = 24$ and 70.

the impedance responses of these two circuit nodes with $C_J = 1.2nF$ (belonging to coexistence phase II) given by Fig. 5(c) show the contrastive result of coexistence phase I. It is found that one of the circuit nodes exhibits ($n = 70$) a large-valued impedance peak at 0.42 MHz, as marked by orange line, while the other circuit node ($n = 24$) shows a great number of impedance peaks with small values. These phenomena clearly demonstrate the property of the third regime (coexistence

phase II). Finally, we set the disorder strength of C_J as $2.0nF$ and measure the impedance responses, as shown by Fig. 5(d). The large-valued impedance peaks located at frequencies of 0.29 and 0.44 MHz of these two circuit nodes of $n = 24$ and 70 (marked by blue and orange lines) indicate the localization phase. In this case, we have clearly observed non-Abelian Anderson transition from delocalized states to coexistence phases and then to localized states in the pseudospin subspace of $|\downarrow\rangle$.

APPENDIX D: SIMULATION RESULTS OF IMPEDANCE SPECTRA IN 1D NON-ABELIAN AAH CIRCUITS

It is worth noting that, due to the significant lossy effect in the fabricated circuit sample, measured impedance peaks are much wider than that in numerical simulations. Here, we calculate the impedance response of two pseudospin subspaces ($|\uparrow\rangle$ and $|\downarrow\rangle$) with different strengths of disorder based on LTSPICE software, as shown in Fig. 6. Blue and orange lines correspond to simulation results of two different circuit nodes ($n = 24$ and 70). The effective series resistance of inductance set as 10 mΩ. Good consistency between simulations and measurements is obtained. As shown in Fig. 6(a), there are many impedance peaks at different frequencies from 0.30 to 0.50 MHz in both pseudospin subspaces of $|\uparrow\rangle$ and $|\downarrow\rangle$, with $C_J = 0.3nF$, indicating the extension of eigenspectra for the non-Abelian AAH circuit. In addition, the peak values are extremely small, corresponding to the delocalized eigenfields in the designed circuit. These simulation results are consistent with the delocalization phase. Figure 6(b) gives simulation results of the impedance responses with $C_J = 0.8nF$. It is clearly shown that there appears a large-valued impedance peak in the subspace $|\uparrow\rangle$ ($|\downarrow\rangle$) of a circuit node ($n = 24$) marked by the blue line located at 0.42 MHz. Oppositely, the other circuit node ($n = 70$) marked by the orange line shows lots of impedance peaks with small values. These phenomena correspond to the property of coexistence phase I, showing that delocalized and localized eigenstates coexist at
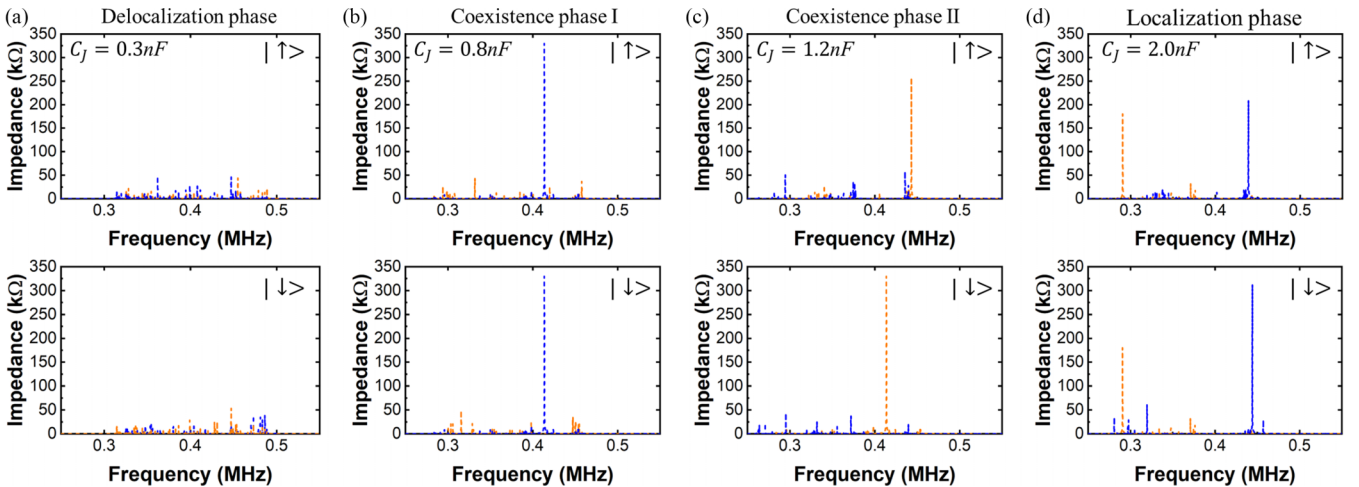
FIG. 6. Simulation results of impedance spectra of 1D non-Abelian Aubry-André-Harper (AAH) circuits in the pseudospin subspace of $|\uparrow\rangle$ and $|\downarrow\rangle$. (a) Simulated impedance responses with $C_J = 0.3nF$, corresponding to the delocalization phase. (b) and (c) Simulated impedance spectra staying in the coexistence phases I and II of the one-dimensional (1D) non-Abelian AAH circuits. The disorder strengths are set as $C_J = 0.8nF$ and $1.2nF$, respectively. (d) Simulated results of impedance response with $C_J = 2.0nF$, corresponding to the localization phase. The blue and orange lines show the simulation results of two different circuit nodes ($n = 24$ and 70).
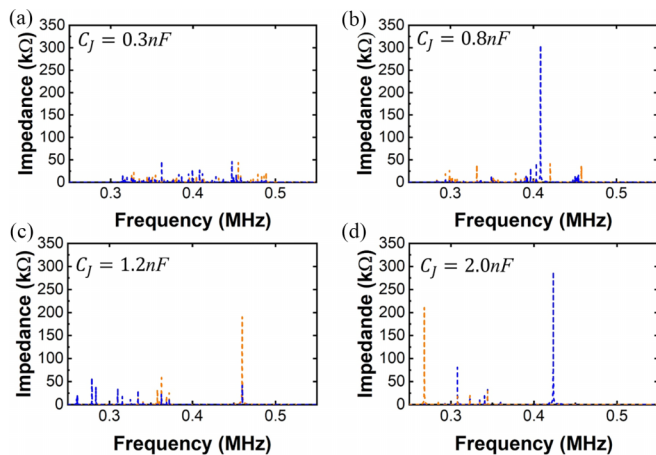
FIG. 7. Simulation results for impedance spectra of $|\uparrow\rangle$ in the non-Abelian Aubry-André-Harper (AAH) circuit with precisely matched quasiperiodic potential. (a)–(d) Simulated impedance responses of the delocalization phase ($C_J = 0.3nF$), coexistence phase I ($C_J = 0.8nF$), coexistence phase II ($C_J = 1.2nF$), and localization phase ($C_J = 2.0nF$).

the same disorder strength. Then we simulate the impedance responses of two circuit nodes with $C_J = 1.2nF$. It is shown that the impedance spectrum of the pseudospin subspace $|\uparrow\rangle$ ($|\downarrow\rangle$) exhibits a large-valued impedance peak at 0.44 MHz (0.42 MHz) when a circuit node ($n = 70$) is excited (the orange line). However, the other circuit node ($n = 24$, illustrated by the blue line) shows many impedance peaks with small values. These results clearly manifest the characteristics of eigenstates in the third regime of coexistence phase II. By further increasing the disorder strength to $C_J = 2.0nF$ (belonging to the localization phase), the measured impedance

spectra of two circuit nodes ($n = 24$ and 70) show the large-valued impedance peaks at only a few frequencies of 0.29 and 0.44 MHz in both pseudospin subspaces ($|\uparrow\rangle$ and $|\downarrow\rangle$), as presented in Fig. 6(d).

From above discussions, we find that impedance responses can display non-Abelian Anderson transition from the delocalization phase to coexistence phases then to the localization phase in fabricated circuits with different strengths of disorder.

To further illustrate the effectiveness on simulating the non-Abelian AAH model with finite-precision capacitances, the impedance spectra of electrical circuits, which precisely match the quasiperiodic distribution, are also simulated, as shown in Figs. 7(a)–7(d). Here, four subplots correspond to results of the delocalization phase ($C_J = 0.3nF$), coexistence phase I ($C_J = 0.8nF$), coexistence phase II ($C_J = 1.2nF$), and localization phase ($C_J = 2.0nF$). It is shown that associated impedance spectra are nearly identical to those in Fig. 6, showing the effectiveness on the implementation of the non-Abelian AAH model with finite-precision capacitances.

APPENDIX E: SIMULATION RESULTS OF VOLTAGE DYNAMICS IN 1D NON-ABELIAN AAH CIRCUITS

In this part, we simulate the temporal dynamics of injected voltage signals with different strengths of disorder. Here, the circuit excitation is in the form of $(V_{1,50_\uparrow} = V_0 e^{i\omega t}, V_{2,50_\uparrow} = -V_0 e^{i\omega t})$ being consistent with the eigenmode of $|\uparrow\rangle_{50}$. The excitation frequencies in different circuits are matched to those of the impedance peaks. Figure 8(a) displays the simulated voltage signal with $C_J = 0.3nF$, and the excitation frequencies at different circuit nodes are 0.35 and 0.45 MHz, respectively. We can clearly see that, under both frequencies, the voltage signals get spread quickly, indicating the
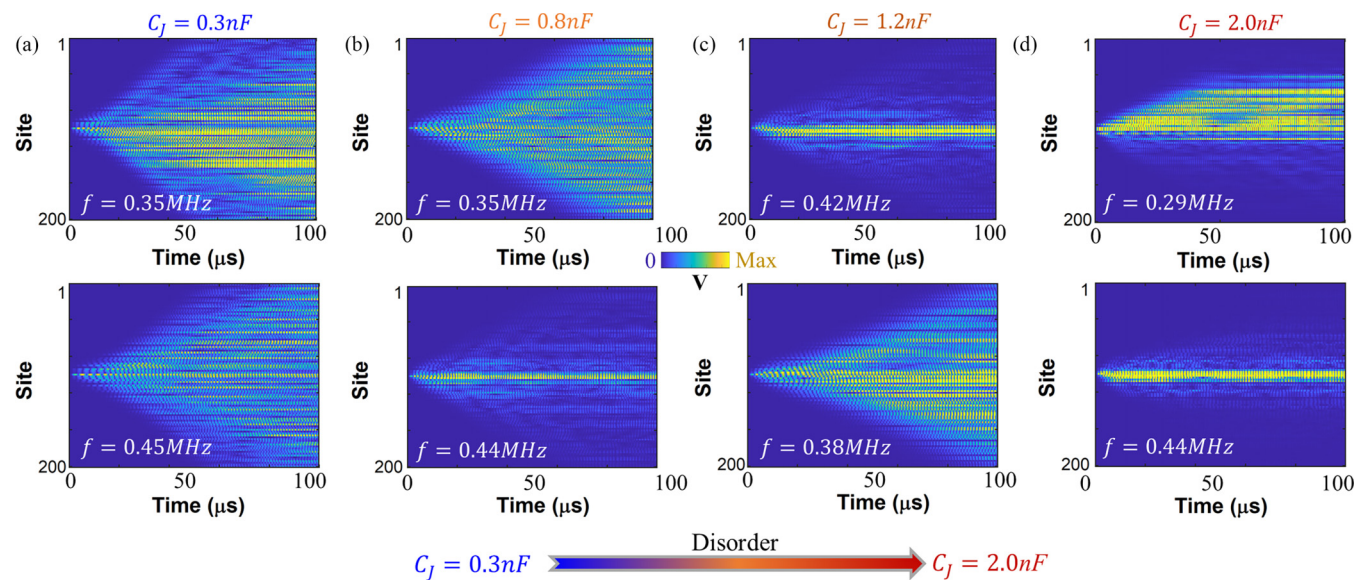
FIG. 8. Simulation results of voltage dynamics in one-dimensional (1D) non-Abelian Aubry-André-Harper (AAH) circuits. (a)–(d) Simulation results of the temporal dynamics at two circuit nodes in the 1D non-Abelian AAH electrical circuits corresponding to the delocalization phase ($C_J = 0.3nF$), the coexistence phase I ($C_J = 0.8nF$), the coexistence phase II ($C_J = 1.2nF$), and the localization phase ($C_J = 2.0nF$), respectively. Here, the circuit excitation is in the form of $[V_{1,50_\uparrow} = V_0 e^{i\omega t}, V_{2,50_\uparrow} = -V_0 e^{i\omega t}]$ being consistent with the eigenmode of $|\uparrow\rangle$ at the 50th lattice site. The excitation frequency is shown in each subplot.

delocalization effect with low disorder strengths. Then we simulate the time dynamics of voltage signal in circuit with $C_J = 0.8nF$, as shown in Fig. 8(b). Under the excitation frequency of 0.35 MHz, the input voltages could exhibit fast-extension behavior, indicating the delocalization effect. Contrary to this result, the injected voltage is localized around the input node with excitation frequency of 0.44 MHz. These results demonstrate the coexistence of delocalization and localization effect, which correspond with the property of coexistence phase I. Furthermore, we set the strength of disorder is set as $1.2nF$, as shown in Fig. 8(c). In this case, the different

circuit nodes are excited by the frequencies of 0.42 and 0.38 MHz. We can clearly observe that the voltage signals localized around the input nodes under the excitation frequency of 0.42 MHz. The voltage signals extend quickly when the excitation frequency is 0.38 MHz. These phenomena clearly manifest the characteristics of eigenstates in the third regime of coexistence phase II. Figure 8(d) presents the voltage evolutions in the circuit with $C_J = 2.0nF$ in simulation. Like the experimental results, the strong localization of voltage signals with excitation frequencies of 0.29 and 0.44 MHz can be clearly observed, corresponding with the localization phase.

---

[1] P. W. Anderson, Phys. Rev. **109**, 1492 (1958).

[2] J. Billy, V. Josse, Z. Zuo, A. Bernard, B. Hambrecht, P. Lugan, D. Clement, L. Sanchez-Palencia, P. Bouyer, and A. Aspect, Nature (London) **453**, 891 (2008).

[3] G. Roati, C. D'Errico, L. Fallani, M. Fattori, C. Fort, M. Zaccanti, G. Modugno, M. Modugno, and M. Inguscio, Nature (London) **453**, 895 (2008).

[4] S. S. Kondov, W. R. McGehee, J. J. Zirbel, and B. DeMarco, Science **334**, 66 (2011).

[5] F. Jendrzejewski, A. Bernard, K. Mueller, P. Cheinet, V. Josse, M. Piraud, L. Pezzé, L. Sanchez-Palencia, A. Aspect, and P. Bouyer, Nat. Phys. **8**, 398 (2012).

[6] G. Semeghini, M. Landini, P. Castilho, S. Roy, G. Spagnolli, A. Trenkwalder, M. Fattori, M. Inguscio, and G. Modugno, Nat. Phys. **11**, 554 (2015).

[7] D. S. Wiersma, P. Bartolini, A. Lagendijk, and R. Righini, Nature (London) **390**, 671 (1997).

[8] T. Schwartz, G. Bartal, S. Fishman, and M. Segev, Nature (London) **446**, 52 (2007).

[9] Y. Lahini, A. Avidan, F. Pozzi, M. Sorel, R. Morandotti, D. N. Christodoulides, and Y. Silberberg, Phys. Rev. Lett. **100**, 013906 (2008).

[10] L. Sapienza, H. Thyrrestrup, S. Stobbe, P. D. Garcia, S. Smolka, and P. Lodahl, Science **327**, 1352 (2010).

[11] A. Schreiber, K. N. Cassemiro, V. Potoček, A. Gábris, I. Jex, and Ch. Silberhorn, Phys. Rev. Lett. **106**, 180403 (2011).

[12] S. Stützer, Y. V. Kartashov, V. A. Vysloukh, A. Tünnermann, S. Nolte, M. Lewenstein, L. Torner, and A. Szameit, Opt. Lett. **37**, 1715 (2012).

[13] M. Segev, Y. Silberberg, and D. N. Christodoulides, Nat. Photon. **7**, 197 (2013).

[14] A. Crespi, R. Osellame, R. Ramponi, V. Giovannetti, R. Fazio, L. Sansoni, F. De Nicola, F. Sciarrino, and P. Mataloni, Nat. Photon. **7**, 322 (2013).

[15] C. Cedzich, T. Rybár, A. H. Werner, A. Alberti, M. Genske, and R. F. Werner, Phys. Rev. Lett. **111**, 160601 (2013).

[16] M. Lee, J. Lee, S. Kim, S. Callard, C. Seassal, and H. Jeon, Sci. Adv. **4**, e1602796 (2018).

[17] S. Weidemann, M. Kremer, S. Longhi, and A. Szameit, Nat. Photon. **15**, 576 (2021).

[18] R. L. Weaver, Wave Motion **12**, 129 (1990).

[19] H. Hu, A. Strybulevych, J. H. Page, S. E. Skipetrov, and B. A. van Tiggelen, Nat. Phys. **4**, 945 (2008).

[20] W. Zhang, D. Zou, Q. Pei, W. He, J. Bao, H. Sun, and X. Zhang, Phys. Rev. Lett. **126**, 146802 (2021).

[21] M. Cutler and N. Mott, Phys. Rev. **181**, 1336 (1969).

[22] P. A. Lee and T. V. Ramakrishnan, Rev. Mod. Phys. **57**, 287 (1985).

[23] R. Dalichaouch, J. P. Armstrong, S. Schultz, P. M. Platzman, and S. L. McCall, Nature (London) **354**, 53 (1991).

[24] I. Manai, J.-F. Clément, R. Chicireanu, C. Hainaut, J. C. Garreau, P. Szriftgiser, and D. Delande, Phys. Rev. Lett. **115**, 240603 (2015).

[25] P. Harper, Proc. Phys. Soc. Lond. A **68**, 874 (1955).

[26] S. Aubry and G. André, Ann. Israel Phys. Soc. **3**, 18 (1980).

[27] Y. G. Sinai, J. Stat. Phys. **46**, 861 (1987).

[28] Y. E. Kraus and O. Zilberberg, Nat. Phys. **12**, 624 (2016).

[29] J. B. Sokoloff, Phys. Rep. **126**, 189 (1984).

[30] Y. Lahini, R. Pugatch, F. Pozzi, M. Sorel, R. Morandotti, N. Davidson, and Y. Silberberg, Phys. Rev. Lett. **103**, 013901 (2009).

[31] Y. E. Kraus, Y. Lahini, Z. Ringel, M. Verbin, and O. Zilberberg, Phys. Rev. Lett. **109**, 106402 (2012).

[32] L.-J. Lang, X. Cai, and S. Chen, Phys. Rev. Lett. **108**, 220401 (2012).

[33] S. Ganeshan, K. Sun, and S. Das Sarma, Phys. Rev. Lett. **110**, 180403 (2013).

[34] M. Verbin, O. Zilberberg, Y. E. Kraus, Y. Lahini, and Y. Silberberg, Phys. Rev. Lett. **110**, 076403 (2013).

[35] S. Weidemann, M. Kremer, S. Longhi, and A. Szameit, Nature (London) **601**, 354 (2022).

[36] H. Jiang, L. Lang, C. Yang, S. Zhu, and S. Chen, Phys. Rev. B **100**, 054301 (2019).

[37] Y. Liu, Q. Zhou, and S. Chen, Phys. Rev. B **104**, 024201 (2021).

[38] Z. Xu, X. Xia, and S. Chen, Sci. China: Phys. Mech. Astron. **65**, 227211 (2022).

[39] Q.-B. Zeng and Y. Xu, Phys. Rev. Res. **2**, 033052 (2020).

[40] S. Longhi, Phys. Rev. Lett. **122**, 237601 (2019).

[41] C. N. Yang and R. L. Mills, Phys. Rev. **96**, 191 (1954).

[42] S. Sugawa, F. Salces-Carcoba, A. R. Perry, Y. Yue, and I. B. Spielman, Science **360**, 1429 (2018).

[43] H. Terças, H. Flayac, D. D. Solnyshkov, and G. Malpuech, Phys. Rev. Lett. **112**, 066402 (2014).

[44] L. B. Ma, S. L. Li, V. M. Fomin, M. Hentschel, J. B. Götte, Y. Yin, M. R. Jorgensen, and O. G. Schmidt, Nat. Commun. **7**, 10983 (2016).

[45] A. Gianfrate, O. Bleu, L. Dominici, V. Ardizzone, M. De Giorgi, D. Ballarini, G. Lerario, K. W. West, L. N. Pfeiffer, D. D. Solnyshkov et al., Nature (London) **578**, 381 (2020).

[46] C. E. Whittaker, T. Dowling, A. V. Nalitov, A. V. Yulin, B. Royall, E. Clarke, M. S. Skolnick, I. A. Shelykh, and D. N. Krizhanovskii, Nat. Photon. **15**, 193 (2021).

[47] K. Y. Bliokh and V. D. Freilikher, Phys. Rev. B **74**, 174302 (2006).

[48] M. Fruchart, Y. Zhou, and V. Vitelli, Nature (London) **577**, 636 (2020).

[49] Y. Yang, B. Yang, G. Ma, J. Li, S. Zhang, and C. T. Chan, arXiv:2305.12206.

[50] J. Wu, Z. Wang, Y. Biao, F. Fei, S. Zhang, Z. Yin, Y. Hu, Z. Song, T. Wu, F. Song et al., Nat. Electron. **5**, 635 (2022).

[51] W. Zhang, H. Wang, H. Sun, and X. Zhang, Phys. Rev. Lett. **130**, 206401 (2023).

[52] Y. Chen, R. Zhang, Z. Xiong, Z. Hang, J. Lin, J. Shen, and C. T. Chan, Nat. Commun. **10**, 3125 (2019).

[53] Y. Yang, C. Peng, D. Zhu, H. Buljan, J. D. Joannopoulos, B. Zhen, and M. Soljačić, Science **365**, 1021 (2019).

[54] Q. Wu, A. A. Soluyanov, and T. Bzdusek, Science **365**, 1273 (2019).

[55] Z.-G. Chen, R.-Y. Zhang, C. T. Chan, and G. Ma, Nat. Phys. **18**, 179 (2022).

[56] X.-L. Zhang, F. Yu, Z.-G. Chen, Z.-N. Tian, Q.-D. Chen, H.-B. Sun, and G. Ma, Nat. Photon. **16**, 390 (2022).

[57] E. G. Guan, H. Yu, and G. Wang, Phys. Lett. A **384**, 126152 (2020).

[58] J. Ningyuan, C. Owens, A. Sommer, D. Schuster, and J. Simon, Phys. Rev. X **5**, 021031 (2015).

[59] V. V. Albert, L. I. Glazman, and L. Jiang, Phys. Rev. Lett. **114**, 173902 (2015).

[60] C. H. Lee, S. Imhof, C. Berger, F. Bayer, J. Brehm, L. W. Molenkamp, T. Kiessling, and R. Thomale, Commun. Phys. **1**, 39 (2018).

[61] M. Ezawa, Phys. Rev. B **100**, 075423 (2019).

[62] T. Helbig, T. Hofmann, C. H. Lee, R. Thomale, S. Imhof, L. W. Molenkamp, and T. Kiessling, Phys. Rev. B **99**, 161114 (2019).

[63] Y. Lu, N. Jia, L. Su, C. Owens, G. Juzeliūnas, D. I. Schuster, and J. Simon, Phys. Rev. B **99**, 020302 (2019).

[64] Y. Wang, H. M. Price, B. Zhang, and Y. D. Chong, Nat. Commun. **11**, 2356 (2020).

[65] N. A. Olekhno, E. I. Kretov, A. A. Stepanenko, P. A. Ivanova, V. V. Yaroshenko, E. M. Puhtina, D. S. Filonov, B. Cappello, L. Matekovits, and M. A. Gorlach, Nat. Commun. **11**, 1436 (2020).

[66] T. Helbig, T. Hofmann, S. Imhof, M. Abdelghany, T. Kiessling, L. W. Molenkamp, C. H. Lee, A. Szameit, M. Greiter, and R. Thomale, Nat. Phys. **16**, 747 (2020).

[67] T. Hofmann, T. Helbig, F. Schindler, N. Salgo, M. Brzeziska, M. Greiter, T. Kiessling, D. Wolf, A. Vollhardt, A. Kabai et al., Phys. Rev. Res. **2**, 023265 (2020).

[68] A. Stegmaier, S. Imhof, T. Helbig, T. Hofmann, C. H. Lee, M. Kremer, A. Fritzsche, T. Feichtner, S. Klembt, S. Hofling et al., Phys. Rev. Lett. **126**, 215302 (2021).

[69] A. Chen, H. Brand, T. Helbig, T. Hofmann, S. Imhof, A. Fritzsche, T. KieSsling, A. Stegmaier, L. K. Upreti, T. Neupert et al., Nat. Commun. **14**, 622 (2023).

[70] S. Liu, R. Shao, S. Ma, L. Zhang, O. You, H. Wu, Y. J. Xiang, T. J. Cui, and S. Zhang, Research **2021**, 5608038 (2021).

[71] B. Lv, R. Chen, R. Li, C. Guan, B. Zhou, G. Dong, C. Zhao, Y. Li, Y. Wang, H. Tao et al., Commun. Phys. **4**, 126 (2021).

[72] J. Dong, V. Juričić, and B. Roy, Phys. Rev. Res. **3**, 023056 (2021).

[73] R. Li, B. Lv, H. Tao, J. Shi, Y. Chong, B. Zhang, and H. Chen, Natl. Sci. Rev. **8**, nwaa192 (2021).

[74] T. Kotwal, F. Moseley, A. Stegmaier, S. Imhof, H. Brand, T. Kießling, R. Thomale, H. Ronellenfitsch, and J. Dunkel, Proc. Natl. Acad. Sci. USA **118**, e2106411118 (2021).

[75] D. Zou, T. Chen, W. He, J. Bao, C. H. Lee, H. Sun, and X. Zhang, Nat. Commun. **12**, 7201 (2021).

[76] W. Zhang, H. Yuan, H. Wang, F. Di, N. Sun, X. Zheng, H. Sun, and X. Zhang, Nat. Commun. **13**, 2392 (2022).

[77] W. Zhang, H. Yuan, N. Sun, H. Sun, and X. Zhang, Nat. Commun. **13**, 2937 (2022).

[78] M. D. Ventra, Y. V. Pershin, and C. Chien, Phys. Rev. Lett. **128**, 097701 (2022).

[79] S. S. Yamada, T. Li, M. Lin, C. W. Peterson, T. L. Hughes, and G. Bahl, Nat. Commun. **13**, 2035 (2022).

[80] L. Song, H. Yang, Y. Cao, and P. Yan, Nat. Commun. **13**, 5601 (2022).

[81] W. Zhang, F. Di, X. Zheng, H. Sun, and X. Zhang, Nat. Commun. **14**, 1083 (2023).

[82] H. Hohmann, T. Hofmann, T. Helbig, S. Imhof, H. Brand, L. K. Upreti, A. Stegmaier, A. Fritzsche, T. Müller, U. Schwingenschlögl et al., Phys. Rev. Res. **5**, L012041 (2023).

[83] S. Ganguly and S. K. Maiti, arXiv:2303.15983.

[84] M. Gonçalves, B. Amorim, E. V. Castro, and P. Ribeiro, SciPost Phys. **13**, 046 (2022).